IEEE Access
Multidisciplinary | Rapid Review | Open Access Journal

Received August 12, 2020, accepted August 27, 2020, date of publication September 1, 2020, date of current version September 21, 2020.

Digital Object Identifier 10.1109/ACCESS.2020.3020981

Orbital Containment Control Algorithm and Complex Information Topology Design for Large-Scale Cluster of Spacecraft

SHIJIE ZHANG[1], FENGZHI GUO[1], ANHUI ZHANG[2], AND TINGTING ZHANG[1]
[1]Research Center of Satellite Technology, Harbin Institute of Technology, Harbin 150080, China
[2]School of Astronautics, Harbin Institute of Technology, Harbin 150001, China

Corresponding author: Shijie Zhang (sjzhang@hit.edu.cn)

ABSTRACT In order to investigate coordinated orbit control problem for large-scale cluster flight spacecraft, a distributed orbital containment control algorithm is proposed for spacecraft cluster flight system with multiple leaders. At first, a general distributed orbital containment control strategy for large-scale cluster spacecraft system is given, so that all followers are driven to the convex hull formed by leaders. Then the constraints of convergence and convergence rate of cluster spacecraft system on control gains and information topology are investigated. Specifically, the control gains which achieve maximal convergence rate are analyzed. Furthermore, two kinds of cell partitions from graph theory are employed to investigate the influence of information topology on steady states of followers, which provides theoretical basis for collision avoidance design. Finally, simulation results show that the designed information topology could meet the requirements of large-scale cluster system, and followers belonging to the same cell have the same steady states.

INDEX TERMS Large-scale cluster, orbital control, multiple leaders, containment control, graph theory, topology design.

I. INTRODUCTION

Cluster flight spacecraft has received growing attention in the recent years [1], [2] for its advantages of greater flexibility, faster response, higher reliability, lower cost and better reconfigurability [3]. Contrary to spacecraft formation flight, cluster flight does not impose strict limits on the geometry of the cluster, and is hence more suitable for implementation by multiple micro-spacecraft. Typically, the inter-spacecraft distances are kept bounded in cluster flight, ranging from several kilometres to hundreds of kilometres [4]. Large-scale cluster spacecraft has been deployed by many institutes, such as ANTS [5], Breakthrough Star Shot project [6], Smart Dust [7] and so on.

Several technical barriers need to be broken down to pave the way for large-scale cluster spacecraft to come into being. Coordinated orbit control of large-scale cluster spacecraft has been identified as one of the enabling technologies. Although there has been lots of results on coordinated control problem for multiple spacecraft systems, we note that most of the existing researches consider leaderless [8], [9] or one leader case [10], [11] where there exists no group objective or only a single group objective.

However, the presence of multiple leaders are more attractive for large-scale cluster system, owing to the fact that such strategies provide attractive solutions to large-scale cluster problems, both in terms of complexity and computational load. As a kind of extended consensus problem, the case with multiple leaders is what we call containment control [12]. The objective of containment control is to guarantee that all the followers asymptotically converge into the convex hull formed by the leaders through information interaction and coordinated control. The containment control problem received significant research interest due to its various applications, such as mobile robots [13], unmanned aerial vehicles(UAVs) [14], underwater vehicles [15] and satellite formation systems [16], [17] etc.

By now, the researches on distributed containment control mainly include first-order systems [13], [18], [19] second-order systems [20]–[21], linear systems [13], [18], [19], nonlinear systems [16], [20], [23], [24] homogeneous and heterogeneous multi-agent systems [26].

The associate editor coordinating the review of this manuscript and approving it for publication was Huaqing Li.

In view of information topology, fixed network topology [16], [20], [23], [24] and switching network topology [19], undirected graph [21] and directed graph [18], [24] are considered. In many researches, containment control is combined with other novel control algorithms, such as finite-time control [15], [16], [23] adaptive control [15], [17] neural network [17], event-triggered control [27], etc. In addition, other problems such as time delay [12], [22] model uncertainties [16], [17], [24] external disturbances [16], [17] are also discussed.

Recently, distributed containment control strategies have gained increased attention in spacecraft control community. In [25], an attitude containment control algorithm was proposed in the case of undirected angle information topology and directed angular velocity information topology, and the case of unavailable relative angle velocity was investigated. Under directed topology, [16] investigated distributed finite-time configuration containment control problem for satellite formation with model uncertainties and perturbations. Moreover, a continuous containment control protocol was proposed for formation satellites modeled by EL equations in [17]. Based on the approximation ability of neural network(NN) and adaptive gain techniques, the model uncertainties and disturbances were compensated for.

Although various novel containment control strategies have been investigated for satellite formation, which enables formation members to converge to the convex hull formed by leaders with a faster convergence rate. Little attention has been paid to the relationship between system performance and information topology design of large-scale cluster system.

On the basis of ensuring wireless energy and information transmission during cluster flight, members must satisfy certain distance constraints to avoid collisions. [28] employed the potential functions methodology to realize collision-avoidance and communication maintaining. However, control force with this method will become larger when the members collide or lose the ability to interact with each other, which is not suitable for large-scale cluster micro-satellite system with limited thrust.

This paper studies orbital containment control problem of large-scale cluster spacecraft from the perspective of cluster information topology. The effects of information topology design on convergence, convergence rate and steady state distribution of each member are analyzed, providing guidance for topology design under various mission requirements. Initially, a general distributed orbital containment control algorithm is proposed to drive followers asymptotically enter into convex full formed by leaders. Furthermore, the influence of information topology and control gain coefficients on system convergence and convergence rate under undirected graph and directed graph has been analyzed respectively. Besides, state distribution of large-scale cluster spacecraft is analyzed based on information topology, which provides a theoretical basis for collision avoidance design of cluster spacecraft. At last, numerical simulation is conducted to verify the influence of information topology design on control performance and collision avoidance of cluster system.

The remainder of this paper is organized as follows: Missions scenarios, algebraic graph theory, orbit dynamics and preliminaries of containment control are briefly given in Section 2. In Section 3, orbital containment control algorithm is proposed for large-scale cluster spacecraft. Then the influence of control gain coefficients and information topology on convergence and convergence rate is derived. State distribution analysis of large-scale cluster spacecraft based on information topology structure design is given in Section 4, providing theoretical foundation for collision avoidance. Numerical simulations to verify the effectiveness of the proposed control algorithm and concluding comments are completed in Section 5 and Section 6, respectively.

II. PRELIMINARIES AND PROBLEM FORMULATION

In this section, some problem descriptions about mission scenarios are introduced, and then preliminary knowledge about graph theory and containment control model are given.

A. MISSION SCENARIOS

Three typical large-scale cluster spacecraft mission scenarios which are closely related to orbit containment control are firstly given and analyzed as follows.

1) LEADER-FOLLOWER COORDINATED ORBITAL CONTROL FOR LARGE-SCALE CLUSTER MICRO-SATELLITE

Large-scale cluster satellite system with leader-follower architecture forms a completed and reliable deep space exploration system [5]. Consists of hundreds of satellites, cluster system need to avoid collisions with asteroids and other objects on orbit. Leaders will autonomously plan a safe area when detect dangerous targets, then cluster members will enter into the safe area through information interaction and coordinated control, while they generally do not require precise final position.

2) COORDINATED ORBITAL CONTROL FOR FRACTIONATED SPACECRAFT

Fractionated spacecraft distributes the functional capabilities of a monolithic spacecraft into multiple free-flying, wirelessly linking modules (service modules and different payloads) [29]. One of the main challenges of this architecture is cluster flight, keeping the various modules within bounded configurations. The fractionated spacecraft generally do not require precise relative orbit and attitude control, as long as the relative distance is within the range of communication and the relative attitude control enables pointing of power transmission links [30].

3) COORDINATED ORBITAL CONTROL FOR GRANULAR SPACECRAFT

Granular spacecraft are complex systems composed of a spatially disordered distribution of a large number of elements, for instance a cloud of grains in orbit [31]. An example of application is a large ultralight optical system, which deploys thousands of high area-to-mass ratio spacecraft(which weigh less than 0.1kg) in orbit [32].

Several stages of coordinated orbit control are needed to achieve normal operation of optical system [33]. In coarse control process, satellites are driven into the two-dimensional plane without strict requirements for final position.

There is no precise requirement for final state of system members in aforementioned cluster spacecraft missions. Cluster members are controlled into the target area(constrained by range of measurement, communication and power transmission links, or just configuration requirement of large systems and safe area of obstacle avoidance). Distributed orbital containment control strategy is one of the effective control methods to solve coordinated orbit problems of spacecraft cluster flight.

A common objective for the above large-scale cluster spacecraft mission scenarios is to form a target area using (virtual) leaders, and then control followers into the target area through inter-spacecraft information interaction and coordinated control. Following we present the basic theoretical preliminaries of information interaction and containment control.

B. GRAPH THEORY

Graph theory is introduced as an useful mathematical tool to describe inter-spacecraft information interaction, providing theoretical basis for performance analysis of system.

We consider a spacecraft cluster system consisting n followers and m (virtual) leaders. The followers set and the leaders set are denoted by $F = \{1, \ldots, n\}$ and $L = \{n+1, \ldots n+m\}$, respectively.

Information interaction topology of cluster system can be modeled by a digraph $\mathcal{G} = (V, E)$ with node set $V(\mathcal{G}) = \{1, \ldots, N\}$ denote spacecraft with dynamics or kinematics characteristics and edge set $E(\mathcal{G}) \subseteq V(\mathcal{G}) \times V(\mathcal{G})$ denote inter-spacecraft information interaction. Each edge $(i, j) \in E(\mathcal{G})$ means spacecraft j can access state information from spacecraft i, and spacecraft i is called a neighbor of spacecraft j. The neighbor set $\mathcal{N}_i = \{j \in V(\mathcal{G}) | (j, i) \in E(\mathcal{G})\}$ of spacecraft i is a collection of all the spacecraft from which spacecraft i can access state information. If $(i, j) \in E(\mathcal{G}) \Leftrightarrow (j, i) \in E(\mathcal{G})$, then it is called undigraph, and bidirectional edge (i, j) indicates that spacecraft i and j can access state information from each other.

Two matrices are frequently used to represent interaction topology: adjacency matrix $\boldsymbol{A} = [a_{ij}] \in \mathbf{R}^{N \times N}$ with $a_{ij} \geq 0$, $a_{ij} > 0$ if $(i, j) \in E(\mathcal{G})$. In this paper, we assume that self-edges are not allowed, i.e. $a_{ii} = 0$. And the Laplacian matrix $L = [l_{ij}] \in \mathbf{R}^{N \times N}$ with $l_{ii} = \sum_{(i,j) \in E(\mathcal{G})} a_{ij}$, $l_{ij} = -a_{ij}$, where $i \neq j$.

The system Laplacian matrix $\boldsymbol{L}$ can also be written as block matrix

$$\boldsymbol{L} = \begin{bmatrix} \boldsymbol{L}_F & \boldsymbol{L}_{FL} \\ \mathbf{0} & \mathbf{0} \end{bmatrix}$$

where $\boldsymbol{L}_F$ is $n \times n$ submatrix composed by rows and columns in which the followers of $\boldsymbol{L}$ are located, and it represents information interaction relationship among followers. $\mathcal{G}_F$ denotes followers and information interaction between followers. $\boldsymbol{L}_{FL}$ is $n \times m$ submatrix composed by rows and columns in which the followers and leaders of $\boldsymbol{L}$ are respectively located, and it represents the information flow from leaders to followers.

Several graph theory tools are given to provide theoretical basis for information topology design of cluster system.

Definition 1 [34]: For directed graph $\mathcal{G}$, a k partition π of $V(\mathcal{G})$ is composed of k cells $C_1, \ldots, C_k$ with $C_i \cap C_j = \Phi$, $(i, j = 1, \ldots k, i \neq j)$ and $\cup_{i=1}^{k} C_i = V(\mathcal{G})$. C_j is a neighbor of C_i $(i, j = 1, \ldots k, i \neq j)$ if there exist $i' \in C_i$ and $j' \in C_j$ such that j' is a neighbor of i'.

Definition 2 [35]: Suppose that $\pi = \{C_1, \ldots, C_k\}$ is a k-partition of $V(\mathcal{G})$, if any two distinct vertices in C_i have the same number of neighbors in C_j for all $j \neq i$, then π is called a π^1 partition. In particular, $\pi^1 = \{H_1, \ldots, H_m\}$ denotes the π^1 cell partition containing H_i $(i = 1, \ldots, m)$ as m cells of π^1.

Definition 3 [36]: Suppose $\pi = \{C_1, \ldots, C_k\}$ is a k-partition of $V(\mathcal{G})$, if for each vertex in C_i, it has the same number of neighbors in all neighbor cells of C_i $(i = 1, \ldots, m)$, then π is called a π^2 partition.

C. CONTAINMENT CONTROL MODEL

The following definitions, assumptions and lemmas related to containment control strategy are needed to derive the main results of this paper.

1) CONVEX FULL

There may exist multiple leaders in large-scale cluster spacecraft missions, and all followers are required to enter into a target area instead of reaching a certain state. Several vertices on the boundary of the target area are selected so that the target area can be approximately replaced by convex polygons which are formed by these vertices [36]. Generally, the more vertices are selected, the higher the approximate accuracy is.

Suppose that the target area (moving or stationary) can be approximated by a convex hull formed by m vertices. Treating these m vertices as (virtual)leaders.

The definition of convex hull is given as follows.

Definition 4 [24]: Let $\mathcal{C}$ be a set in a real vector space $V \subseteq \boldsymbol{R}^p$. The set $\mathcal{C}$ is convex if, for any x and y in $\mathcal{C}$, the point $(1-t)x + ty \in \mathcal{C}$ for any $t \in [0, 1]$. The convex hull for a set of points $X = \{x_1, \ldots, x_m\}$ in V is the minimal convex set containing all points in X. We use $CO(X)$ to denote the

convex hull of X. In particular, $CO(X) = \{\sum_{i=1}^{m} \alpha_i x_i | x_i \in X, \alpha_i \in \boldsymbol{R}, \alpha_i \geq 0, \sum_{i=1}^{m} \alpha_i = 1\}$

Remark 1: Vertices information of target area could be provided by earth station or be autonomously generated by cluster spacecraft which have strong sense, communication and information processing capability. Once the convex hull which approximates the target area is selected, vertices information of the convex hull can be seen as virtual leaders of the cluster system, while cluster members are regarded as followers. Leaders form a static or dynamic convex full, and followers are driven to the convex hull formed by leaders through inter-spacecraft information interaction and coordinated control. Thus coordinated orbit control problem of large-scale cluster spacecraft is transformed into orbit containment control problem of spacecraft cluster with multiple leaders.

2) DISTRIBUTED ORBITAL CONTAINMENT CONTROL FORMULATION

To simplify controller design and analysis, we assume that for any $i \in L, \dot{\boldsymbol{r}}_i = \boldsymbol{0}$, which means the target area formed by leaders is stationary relative to the reference frame. That is, the position of leaders remains unchanged during control process. So orbit motion of leaders in reference frame could be written as $\ddot{\boldsymbol{r}}_i = \boldsymbol{0}, i \in L$.

Orbit dynamics of followers $i \in F$ with respect to the LVLH coordinate frame can be written as

$$\begin{aligned} &\ddot{x}_i - 2\omega\dot{y}_i - 3\omega^2 x_i = u_{x_i} \\ &\ddot{y}_i + 2\omega\dot{x}_i = u_{y_i} \qquad (i = 1, \ldots, n) \\ &\ddot{z}_i + \omega^2 z_i = u_{z_i} \end{aligned} \tag{1}$$

where $\boldsymbol{r}_i = \begin{bmatrix} x_i & y_i & z_i \end{bmatrix}^T$, $\dot{\boldsymbol{r}}_i = \begin{bmatrix} \dot{x}_i & \dot{y}_i & \dot{z}_i \end{bmatrix}^T$, $\ddot{\boldsymbol{r}}_i = \begin{bmatrix} \ddot{x}_i & \ddot{y}_i & \ddot{z}_i \end{bmatrix}^T$ denote the relative position, relative velocity and accelerated velocity of follower i to the reference spacecraft, respectively. $\boldsymbol{u}_i = \begin{bmatrix} u_{x_i} & u_{y_i} & u_{z_i} \end{bmatrix}^T$ denotes the control input.

Our aim in this paper is to propose appropriate distributed control algorithm for the followers (i.e., those indexed from 1 to n), so that in an asymptotic manner, they can travel into the convex hull formed by the leaders(i.e., those spacecraft indexed from $n+1$ to $n+m$). We will also analyze under what conditions the containment behaviors can be guaranteed and perform rigorous convergence and convergence rate analysis accordingly. On this basis, the influence of information topology design on steady state distribution of followers is analyzed, which provides a theoretical reference for collision avoidance of cluster members.

In this paper, there is no information interaction between leaders. The trajectory of leaders is not affected by other members, while followers need generate control instructions with neighbors' information. In order to ensure that all the followers enter the convex hull formed by leaders, it must be ensured that the motion of any follower can be affected by leaders directly or indirectly. Otherwise, there will exist followers whose motion is not affected by any leader, nor will converge to the convex hull formed by the leaders. Thus the information topology of cluster needs to meet the following conditions.

Assumption 1 [21]: Suppose that for each follower i, there exists at least one leader j that has a path to the follower i.

Lemma 1 [21]: If Assumption 1 holds, and the information interaction between followers are bidirectional, then $\boldsymbol{L}_F$ is symmetric positive definite matrix, each entry of $-\boldsymbol{L}_F^{-1}\boldsymbol{L}_{FL}$ is nonnegative and each row sum of $-\boldsymbol{L}_F^{-1}\boldsymbol{L}_{FL}$ is equal to $\boldsymbol{1}$.

Consensus control protocol for followers could be written in the following form

$$\boldsymbol{u}_i = f\left(\boldsymbol{r}_F, \dot{\boldsymbol{r}}_F, \boldsymbol{r}_L, \dot{\boldsymbol{r}}_L\right), \quad i \in F$$

where

$$\begin{aligned} &\boldsymbol{r}_F = \left[\boldsymbol{r}_1^T, \ldots, \boldsymbol{r}_n^T\right]^T, \quad \dot{\boldsymbol{r}}_F = \left[\dot{\boldsymbol{r}}_1^T, \ldots, \dot{\boldsymbol{r}}_n^T\right]^T, \\ &\boldsymbol{r}_L = \left[\boldsymbol{r}_{n+1}^T, \ldots, \boldsymbol{r}_{n+m}^T\right]^T, \quad \dot{\boldsymbol{r}}_L = \left[\dot{\boldsymbol{r}}_{n+1}^T, \ldots, \dot{\boldsymbol{r}}_{n+m}^T\right]^T. \end{aligned}$$

According to Definition 4 and Lemma 1, the convex weighted average of the leader's position and velocity is

$$\begin{aligned} \boldsymbol{r}_d &= -\left(\boldsymbol{L}_F^{-1}\boldsymbol{L}_{FL} \otimes \boldsymbol{I}_3\right)\boldsymbol{r}_L \\ \dot{\boldsymbol{r}}_d &= -\left(\boldsymbol{L}_F^{-1}\boldsymbol{L}_{FL} \otimes \boldsymbol{I}_3\right)\dot{\boldsymbol{r}}_L \end{aligned}$$

$\boldsymbol{r}_d$ and $\dot{\boldsymbol{r}}_d$ respectively represent the desired position and desired velocity of followers.

Furthermore, the velocity of leaders relative to reference frame is $\dot{\boldsymbol{r}}_L = \boldsymbol{0}$, that is $\dot{\boldsymbol{r}}_d = \boldsymbol{0}$. Then the desired position and desired velocity of followers could be also written as

$$\begin{aligned} \boldsymbol{r}_d &= -\left(\boldsymbol{L}_F^{-1}\boldsymbol{L}_{FL} \otimes \boldsymbol{I}_3\right)\boldsymbol{r}_L \\ \dot{\boldsymbol{r}}_d &= \boldsymbol{0} \end{aligned}$$

Control force $\boldsymbol{u}_i$ is used to solve orbit containment control problem with multiple leader-follower structure. The position of followers(from 1 to n) asymptotically enter into the convex hull formed by leaders (from $n+1$ to m), and velocity converge to 0 from any initial state. That is $\lim_{t\to\infty} \|\boldsymbol{r}_i(t) - \boldsymbol{r}_d(t)\| = 0$, $\lim_{t\to\infty} \dot{\boldsymbol{r}}_i = 0, \forall i \in F$. Then we say it has achieved orbital containment control of large-scale cluster of spacecraft.

III. DISTRIBUTED ORBITAL CONTAINMENT CONTROL BASED ON INFORMATION TOPOLOGY DESIGN

In this section, the distributed orbital containment control problem of large-scale cluster spacecraft based on topology is investigated. The containment control problem will be investigated in two aspects, respectively: 1) Parameter design of orbital containment controller, 2) Convergence and convergence rate analysis. The study will provide a general orbital containment control method for large-scale cluster flight spacecraft and theoretical reference for how to obtain a satisfactory convergence rate using less control force and simpler information topology design.

A. ORBITAL CONTAINMENT CONTRL STRUCTURE DESIGN AND CONVERGENCE ANALYSIS

In order to realize orbit containment control of large-scale cluster spacecraft, the members are required to track the desired position $\boldsymbol{r}_d$ and desired velocity $\dot{\boldsymbol{r}}_d$, meanwhile it maintains a certain formation configuration during control process. Based on consensus theory and Ref. [21], a general orbital containment control algorithm is given for followers of large-scale cluster, so that followers can exponentially converge to the stationary convex hull formed by leaders under complex topology.

1) DISTRIBUTED ORBITAL CONTAINMENT CONTROLLER

In order to analyse the influence of information topology on system performance, a general distributed orbital containment control method based on local information interaction is given: each spacecraft generates its own control protocol based on its own absolute state information and relative state information of its neighbours.

$$\begin{aligned}
u_{x_i} &= -3\omega^2 x_i - 2\omega\dot{y}_i - \alpha\dot{x}_i - \sum_{j\in N_i} a_{ij}[\gamma_0(x_i - x_j) + \gamma_1(\dot{x}_i - \dot{x}_j)] \\
u_{y_i} &= 2\omega\dot{x}_i - \alpha\dot{y}_i - \sum_{j\in N_i} a_{ij}[\gamma_0(y_i - y_j) + \gamma_1(\dot{y}_i - \dot{y}_j)] \\
u_{z_i} &= \omega^2 z_i - \alpha\dot{z}_i - \sum_{j\in N_i} a_{ij}[\gamma_0(z_i - z_j) + \gamma_1(\dot{z}_i - \dot{z}_j)] \qquad (2)
\end{aligned}$$

a_{ij} is the (i, j) entry of the adjacency matrix $\boldsymbol{A}$ which associated with the graph $\mathcal{G}$. If the ith spacecraft can access state information from the jth spacecraft, $a_{ij} = 1$, else $a_{ij} = 0$. Control gain coefficients $\alpha, \gamma_0, \gamma_1$ respectively represent absolute velocity, relative position and relative velocity feedback term weight.

Remark 2: Distributed orbital containment controller (2) mainly consists of two parts: absolute motion control term and relative motion control term. The controller has a very clear structure. $[-3\omega^2 x_i - 2\omega\dot{y}_i - \alpha\dot{x}_i, 2\omega\dot{x}_i - \alpha\dot{y}_i, \omega^2 z_i - \alpha\dot{z}_i]^T$ is absolute motion control term, and the absolute motion represents the state of followers relative to the reference frame. $-\sum_{j\in\mathcal{N}_i} a_{ij}[\gamma_0(\boldsymbol{r}_i - \boldsymbol{r}_j) + \gamma_1(\dot{\boldsymbol{r}}_i - \dot{\boldsymbol{r}}_j)]$ is relative motion control feedback term. Relative motion control is used to control relative position and relative velocity between cluster spacecraft, which makes the cluster composed of multiple independent spacecraft more integrated. Where relative position control feedback term $-\sum_{j\in\mathcal{N}_i} a_{ij}\gamma_0(\boldsymbol{r}_i - \boldsymbol{r}_j)$ is necessary in containment controller design for the needs of driving followers into the convex hull formed by leaders, that is $\gamma_0 > 0$. Relative velocity control term $-\sum_{j\in\mathcal{N}_i} a_{ij}\gamma_1(\dot{\boldsymbol{r}}_i - \dot{\boldsymbol{r}}_j)$ is used to drive relative velocity between neighbours to the desired state. Relative motion control term could improve control performance and reliability of the whole cluster system.

Remark 3: The distributed characteristics of large-scale cluster spacecraft orbital containment control strategy (2) are mainly reflected from the following aspects: 1) For the ith follower, $\boldsymbol{u}_i$ is composed of its own and neighbors' information. 2) Neighbors' relative position and velocity information can be obtained by measuring elements on satellites. 3) Neighbors' controller information can be obtained by communication equipments among satellites.

Remark 4: For large-scale cluster spacecraft system, the control input $\boldsymbol{u}_i$ are produced by thrusters. In practical engineering, it is necessary to consider the output saturation of the thrusters, which is discussed in numerical simulations.

According to controller (2), the motion of each follower is affected by its neighbors, so control performance of the whole cluster system is closely related to the cluster information topology.

Since the neighbor spacecraft set of cluster members is not limited in controller (2), a general cluster information topology is considered instead of a specific ring or tree structure. Thus, cluster information topology is a quantity that can be designed according to the requirements of cluster control performance.

2) CONVERGENCE ANALYSIS

Theorem 1 and Theorem 2 will give convergence analysis for orbital containment control of large-scale cluster system without considering external disturbances, model uncertainties, time delay, etc.

Substituting controller (2) into dynamics equation (1), it can be obtained that

$$\begin{aligned}
\begin{bmatrix} \dot{\boldsymbol{r}}_F \\ \ddot{\boldsymbol{r}}_F \end{bmatrix} &= \begin{bmatrix} \boldsymbol{0} & \boldsymbol{I}_n \otimes \boldsymbol{I}_3 \\ -\gamma_0 L_F \otimes \boldsymbol{I}_3 & -(\alpha \boldsymbol{I}_n + \gamma_1 L_F) \otimes \boldsymbol{I}_3 \end{bmatrix} \begin{bmatrix} \boldsymbol{r}_F \\ \dot{\boldsymbol{r}}_F \end{bmatrix} \\
&\quad + \begin{bmatrix} \boldsymbol{0} & \boldsymbol{0} \\ -\gamma_0 L_{FL} \otimes \boldsymbol{I}_3 & -\gamma_1 L_{FL} \otimes \boldsymbol{I}_3 \end{bmatrix} \begin{bmatrix} \boldsymbol{r}_L \\ \dot{\boldsymbol{r}}_L \end{bmatrix} \qquad (3)
\end{aligned}$$

where

$$\boldsymbol{\Gamma} = \begin{bmatrix} \boldsymbol{0} & \boldsymbol{I}_n \otimes \boldsymbol{I}_3 \\ -\gamma_0 L_F \otimes \boldsymbol{I}_3 & -(\alpha \boldsymbol{I}_n + \gamma_1 L_F) \otimes \boldsymbol{I}_3 \end{bmatrix} \qquad (4)$$

Let the initial position and initial velocity of followers are $\boldsymbol{r}_F(0)$ and $\dot{\boldsymbol{r}}_F(0)$ respectively, then integrating (3), we can get

$$\begin{aligned}
&\begin{bmatrix} \boldsymbol{r}_F \\ \dot{\boldsymbol{r}}_F \end{bmatrix} \\
&= \mathrm{e}^{\boldsymbol{\Gamma} t} \begin{bmatrix} \boldsymbol{r}_F(0) \\ \dot{\boldsymbol{r}}_F(0) \end{bmatrix} \\
&\quad + \int_0^t \mathrm{e}^{\boldsymbol{\Gamma}(t-\tau)} d\tau \begin{bmatrix} \boldsymbol{0} & \boldsymbol{0} \\ -\gamma_0 L_{FL} \otimes \boldsymbol{I}_3 & -\gamma_1 L_{FL} \otimes \boldsymbol{I}_3 \end{bmatrix} \begin{bmatrix} \boldsymbol{r}_L \\ \dot{\boldsymbol{r}}_L \end{bmatrix} \\
&= \mathrm{e}^{\boldsymbol{\Gamma} t} \begin{bmatrix} \boldsymbol{r}_F(0) \\ \dot{\boldsymbol{r}}_F(0) \end{bmatrix} + (\mathrm{e}^{\boldsymbol{\Gamma} t} \boldsymbol{\Gamma}^{-1} - \boldsymbol{\Gamma}^{-1}) \begin{bmatrix} \boldsymbol{0} \\ (-\gamma_0 L_{FL} \otimes \boldsymbol{I}_3) \boldsymbol{r}_L \end{bmatrix} \qquad (5)
\end{aligned}$$

Theorem 1: If ***Assumption 1*** holds, then followers can be driven into convex full formed by leaders asymptotically using orbit containment controller (2) if and only if all eigenvalues of $\boldsymbol{\Gamma}$ have negative real parts.

Proof:

a: SUFFICIENCY

Since all eigenvalues of $\mathbf{\Gamma}$ have negative real parts, then $\mathbf{e}^{\Gamma t} \to 0$, it can be obtained that

$$\begin{bmatrix} \boldsymbol{r}_F(t) \\ \dot{\boldsymbol{r}}_F(t) \end{bmatrix} \to -\mathbf{\Gamma}^{-1} \begin{bmatrix} \mathbf{0} \\ -\left(\gamma_0 L_{FL} \otimes \boldsymbol{I}_3\right) \boldsymbol{r}_L \end{bmatrix} \tag{6}$$

It can be calculated that

$$\begin{aligned} &\mathbf{\Gamma}^{-1} \\ &= \begin{bmatrix} -\left(\frac{\alpha}{\gamma_0} L_F^{-1} + \frac{\gamma_1}{\gamma_0} \boldsymbol{I}_n\right) \otimes \boldsymbol{I}_3 & -\left(\gamma_0 L_F \otimes \boldsymbol{I}_3\right)^{-1} \\ \boldsymbol{I}_n \otimes \boldsymbol{I}_3 & \mathbf{0} \end{bmatrix} \\ &\quad -\mathbf{\Gamma}^{-1} \begin{bmatrix} \mathbf{0} \\ -\left(\gamma_0 L_{FL} \otimes \boldsymbol{I}_3\right) \boldsymbol{r}_L \end{bmatrix} \end{aligned} \tag{7}$$

$$= \begin{bmatrix} -\left(L_F^{-1} L_{FL} \otimes \boldsymbol{I}_3\right) \boldsymbol{r}_L \\ \mathbf{0} \end{bmatrix} \tag{8}$$

Furthermore

$$\lim_{t \to \infty} \begin{bmatrix} \boldsymbol{r}_F(t) \\ \dot{\boldsymbol{r}}_F(t) \end{bmatrix} \to \begin{bmatrix} -\left(L_F^{-1} L_{FL} \otimes \boldsymbol{I}_3\right) \boldsymbol{r}_L \\ \mathbf{0} \end{bmatrix} \tag{9}$$

That is, followers enter the convex hull formed by the leaders asymptotically. And the velocity of followers converges to $\boldsymbol{0}$ relative to reference frame.

b: NECESSITY

If there exists an eigenvalue λ of $\mathbf{\Gamma}$, satisfies $\mathrm{Re}\,(\lambda) \geq 0$, then $\mathrm{e}^{\Gamma t} \nrightarrow 0$. Therefore, it can not be guaranteed that for any initial value $\boldsymbol{r}_F(0)$ and $\dot{\boldsymbol{r}}_F(0)$, $\begin{bmatrix} \boldsymbol{r}_F(t) \\ \dot{\boldsymbol{r}}_F(t) \end{bmatrix} \to \begin{bmatrix} -\left(L_F^{-1} L_{FL} \otimes I_3\right) \boldsymbol{r}_L \\ \mathbf{0} \end{bmatrix}$ holds on. This contradicts controller (2) achieving containment control asymptotically.

Now Theorem 1 has been proved.

It will be proved in Theorem 2 that all followers can converge to the convex hull formed by leaders with exponential convergence rate.

To facilitate convergence analysis, state variables are introduced

$$\boldsymbol{\eta} = \boldsymbol{\xi}_F + \boldsymbol{Q} \boldsymbol{\xi}_L \tag{10}$$

where $\boldsymbol{\xi}_F = \begin{bmatrix} \boldsymbol{r}_F^T & \dot{\boldsymbol{r}}_F^T \end{bmatrix}^T$, $\boldsymbol{\xi}_L = \begin{bmatrix} \boldsymbol{r}_L^T & \dot{\boldsymbol{r}}_L^T \end{bmatrix}^T$, $\boldsymbol{Q} = \mathbf{\Gamma}^{-1} \begin{bmatrix} 0 & 0 \\ -\gamma_0 \boldsymbol{L}_{FL} \otimes \boldsymbol{I}_3 & \gamma_1 \boldsymbol{L}_{FL} \otimes \boldsymbol{I}_3 \end{bmatrix}$. Then it can be derived that $\dot{\boldsymbol{\eta}} = \mathbf{\Gamma} \boldsymbol{\eta}$.

Theorem 2: If Assumption 1 holds, and all eigenvalues of state matrix $\mathbf{\Gamma}$ have negative real parts. Then under the control of orbital containment control algorithm (2), all followers of cluster system will enter into the convex full formed by leaders with exponential convergence rate. Moreover $\lim_{t \to \infty} \boldsymbol{r}_F \to -\boldsymbol{L}_F^{-1} \boldsymbol{L}_{FL} \boldsymbol{r}_L$, $\lim_{t \to \infty} \dot{\boldsymbol{r}}_F \to \mathbf{0}$.

Proof: Consider the following Lyapunov candidate

$$V = \frac{1}{2} \boldsymbol{\eta}^2 \tag{11}$$

Taking the derivative of Eq.(11)

$$\begin{aligned} \dot{V} &= \boldsymbol{\eta} \dot{\boldsymbol{\eta}} \\ &= \mathbf{\Gamma} \boldsymbol{\eta}^2 \\ &= \frac{1}{2} \boldsymbol{\eta}^T \left(\mathbf{\Gamma} + \mathbf{\Gamma}^T\right) \boldsymbol{\eta} \end{aligned} \tag{12}$$

All eigenvalues of $\mathbf{\Gamma}$ have negative real parts, the maximum eigenvalue is denoted as $\lambda_{\max}(\mathbf{\Gamma}) < 0$, then we can obtain

$$\dot{V} = \boldsymbol{\eta}^T \mathbf{\Gamma} \boldsymbol{\eta} \leq \lambda_{\max}(\mathbf{\Gamma}) \|\boldsymbol{\eta}\|^2 < 0 \tag{13}$$

It can be seen that $\dot{V} \leq 0$, the cluster system can asymptotically converge to the target area.

Then the Eq.(13) can be rewritten as

$$\frac{dV}{dt} - 2\lambda_{\max}(\mathbf{\Gamma}) V \leq 0 \tag{14}$$

Integrating equation (14) and we can obtain

$$V(\boldsymbol{\eta}(t)) \leq V(\boldsymbol{\eta}_0) e^{2\lambda_{\max}(\mathbf{\Gamma}) t} \tag{15}$$

According to (11), we can obtain

$$\|\boldsymbol{\eta}(t)\| \leq \|\boldsymbol{\eta}_0\| e^{\lambda_{\max}(\mathbf{\Gamma}) t} \tag{16}$$

Because $\lambda_{\max}(\mathbf{\Gamma}) < 0$, we can get $e^{\lambda_{\max}(\mathbf{\Gamma}) t} \to 0$. The system satisfies the conditions of exponential convergence, and $\lim_{t \to \infty} \boldsymbol{\eta}(t) \to \mathbf{0}$.

Then $\lim_{t \to \infty} \boldsymbol{r}_F = -\left(\boldsymbol{L}_F^{-1} \boldsymbol{L}_{FL} \otimes \boldsymbol{I}_3\right) \boldsymbol{r}_L$, $\lim_{t \to \infty} \dot{\boldsymbol{r}}_F = \mathbf{0}$.

In a word, all followers will exponentially converge to the convex hull formed by leaders. As can be seen, the orbital containment control algorithm (2) can make the position and velocity of the system decay exponentially, and exponential convergence rate is $a \geq -\lambda_{\max}(\mathbf{\Gamma})$.

Now Theorem 2 has been proved.

B. CONTROL GAIN COEFFICIENT DESIGN

1) CONVERGENCE CONSTRAINTS

It can be concluded from Theorem 1 that followers can be driven into convex full formed by leaders if and only if all eigenvalues of $\mathbf{\Gamma}$ have negative real parts. Eigenvalue distribution of $\mathbf{\Gamma}$ depends on information topology $\mathcal{G}$ of cluster system and control gain coefficients α, γ_0, γ_1 . As can be seen, convergence, convergence rate of cluster system are closely related with information topology and control gain coefficients. Whereas eigenvalues structure of the Laplacian matrix is actually an algebraic representation of cluster system's information topology structure. In the following we will analyze the influence of information topology structure and control gain coefficients on convergence and convergence rate, providing a way to obtain better control performance with less communication/measurement pressure.

Theorem 3: If ***Assumption* 1** holds, then under the action of orbital containment controller (2), followers can be driven

into convex full formed by leaders asymptotically if and only if

$$\begin{aligned} \alpha &> \max_i(p_i\gamma_1) \\ 0 &> \max\left(\frac{\gamma_0^2 q_i^2}{(\alpha - p_i\gamma_1)^2} - \frac{\gamma_0\gamma_1 q_i^2}{\alpha - p_i\gamma_1} + p_i\gamma_0\right) \end{aligned} \tag{17}$$

where $\mu_i\,(i = 1, \ldots, n)$ are eigenvalues of $\boldsymbol{L}_F$. $p_i = \mathrm{Re}\{\mu_i\}$, $q_i = Im\{\mu_i\}$.

Proof: Let eigenvalues of $\boldsymbol{\Gamma}$ are $\lambda_i\ (i = 1, \ldots, n)$, then polynomial $f_{\mu_i}(\lambda_i) = (\lambda_i)^2 + (\alpha - \gamma_1\mu_i)\lambda_i - \gamma_0\mu_i$. Eigenvalues of $-L_F$ have negative real numbers according to Lemma 1, suppose that $0 > \mu_1 \geq \mu_2 \geq \ldots \geq \mu_n$.

According to Lemma 2 and Theorem 1 in Ref.[37], we can see that every root of $f_{\mu_i}(\lambda_i)$ lies in the open left-half complex plane if and only if every root of the real coefficient polynomial $f_{\mu_i}(\lambda_i) f_{\bar{\mu}_i}(\lambda_i)$ does, since $f_{\mu_i}(\bar{\lambda}_0) = \overline{f_{\bar{\mu}_i}(\lambda_0)}$ for any complex number λ_0. Let $a_i = \alpha - p_i\gamma_1, b_i = -p_i\gamma_0, c_i = q_i\gamma_1$ and $d_i = q_i\gamma_0$ Then we can get

$$f_{\mu_i}(\lambda_i) f_{\bar{\mu}_i}(\lambda_i) = \lambda_i^4 + a_{1i}\lambda_i^3 + a_{2i}\lambda_i^2 + a_{3i}\lambda_i + a_{4i}$$

where $a_{1i} = 2a_i$, $a_{2i} = a_i^2 + 2b_i + c_i^2$, $a_{3i} = 2a_ib_i + 2c_id_i$, $a_{4i} = b_i^2 + d_i^2$.

According to Hurwitz stability criteria, all the eigenvalues have negative real parts if and only if

$$\Delta_{1i} = 2a_i > 0, \quad \Delta_{2i} = \begin{vmatrix} a_{1i} & 1 \\ a_{3i} & a_{2i} \end{vmatrix} > 0$$

$$\Delta_{3i} = \begin{vmatrix} a_{1i} & 1 & 0 \\ a_{3i} & a_{2i} & a_{1i} \\ 0 & a_{4i} & a_{3i} \end{vmatrix} > 0, \quad \Delta_{4i} = \left(b_i^2 + d_i^2\right)\Delta_{3i} > 0$$

They can be rewritten as

$$a_i > 0, \quad b_i > \frac{c_id_i}{a_i} - a_i^2 - c_i^2$$

$$b_i > \frac{d_i^2}{a_i^2} - \frac{c_id_i}{a_i}, \quad b_i^2 + d_i^2 \neq 0$$

By further calculation, (17) can be derived.

Thus we can obtain that all eigenvalues of $\boldsymbol{\Gamma}$ have negative real parts. Then according to **Theorem 1**, we can conclude that followers asymptotically enter the convex hull formed by the leaders if and only if (17) holds.

The proof has been completed.

Collary 1. If Assumption 1 holds, the flow of information from leaders to followers is unidirectional and information interaction between followers is bidirectional. Thus eigenvalues of $-\boldsymbol{L}_F$ are all negative real numbers. Then, under the action of control protocol (2), followers can be driven into convex full formed by leaders asymptotically if and only if

$$\begin{aligned} \alpha &> \max_i(\mu_i\gamma_1) \\ \gamma_0 &> 0 \end{aligned}$$

Collary 2: If spacecraft i can not measure relative velocity information, that is $\gamma_1 = 0$. Then the sufficient and necessary condition for controller (2) to realize orbital containment control of cluster spacecraft is $\alpha > \max_i \sqrt{\frac{\gamma_0 q_i^2}{-p_i}}$, $\gamma_0 > 0$. If spacecraft i can not measure absolute velocity information, that is $\alpha = 0$. Then the sufficient and necessary condition for controller (2) to realize orbital containment control of cluster spacecraft is $\gamma_0 > 0, \gamma_1 > 0, \gamma_0 q_i^2 + p_i\gamma_1^2\left(p_i^2 + q_i^2\right) < 0$. $(i = 1, 2, \cdots, n)$

2) CONVERGENCE RATE CONSTRAINT

In this subsection, constraints of asymptotic convergence and convergence rate on information links and control gain coefficients under undirected topology are given. There is no information interaction between leaders, and the flow of information from leaders to followers is unidirectional while the flow of information among followers is bidirectional. The control gain coefficients which achieve maximal convergence rate are obtained.

It can be calculated that eigenvalues of $\boldsymbol{\Gamma}$ are

$$\begin{aligned} \lambda_{i1} &= \frac{-(\alpha - \gamma_1\mu_i) + \sqrt{(\alpha - \gamma_1\mu_i)^2 + 4\gamma_0\mu_i}}{2} \\ \lambda_{i2} &= \frac{-(\alpha - \gamma_1\mu_i) - \sqrt{(\alpha - \gamma_1\mu_i)^2 + 4\gamma_0\mu_i}}{2} \ (i = 1, \ldots, n) \end{aligned} \tag{18}$$

Let a be maximum convergence rate of cluster system, then it can be obtained that

$$a = -\max\{\mathrm{Re}\lambda_{ij} | i = 1, \ldots, n; j = 1,\ 2\} \tag{19}$$

Because $\mathrm{Re}\{\lambda_{i1}\} \geq \mathrm{Re}\{\lambda_{i2}\}$, the maximum convergence rate can be written as

$$a = -\max\{\mathrm{Re}\lambda_{i1} | i = 1, \ldots, n\} \tag{20}$$

The second inequality in **Theorem 3** shows that $\gamma_0 \neq 0$. Furthermore, because $p_i = \mathrm{Re}(\mu_i) < 0$, according to the first inequality in Theorem 3, we can let either γ_1 or α be 0 and the other is positive. Therefore, controller (2) must contain relative position information of spacecraft, while relative velocity between neighbor spacecraft and absolute velocity of spacecraft may not be obtained due to failure of sensors or limited communication bandwidth.

In the following, two different cases are investigated respectively:

1) Absence of absolute velocity feedback. If spacecraft i can not measure absolute velocity information of itself, that is $\alpha = 0$.

2) Absence of relative velocity feedback. If spacecraft i can not measure relative velocity information of its neighbors, there does not exist relative velocity feedback term in controller (2), that is $\gamma_1 = 0$. The influence of control gain coefficients on convergence rate under undirected topology can be obtained as Table 1.

According to Eqs. (18)-(20), convergence rate of cluster system under undirected topology is related to minimum nonzero eigenvalue $-\mu_1$ of submatrix $\boldsymbol{L}_F$ corresponding

TABLE 1. The influence of contrl gain coefficients on convergence rate under undirected topology.

Coefficients	Conditions	$(0, p]$	Maximum points p	The maximum value	$(p, +\infty)$
α=0 $\gamma_0 > 0$ $\gamma_1 > 0$	γ_0 is fixed	Monotonically increase	$\gamma_1 = \frac{2\sqrt{-\gamma_0\mu_n}}{\sqrt{-\mu_1(\mu_1-2\mu_n)}}$	$a = \frac{\sqrt{\gamma_0\mu_1\mu_n}}{\sqrt{\mu_1-2\mu_n}}$	Monotonically decrease
	γ_1 is fixed	monotonically increase	$\gamma_0 = \frac{(-\mu_1^2+2\mu_1\mu_n)\gamma_1^2}{-4\mu_n}$	$a = -\frac{\gamma_1\mu_1}{2}$	Remain unchanged
γ_1=0 $\gamma_0 > 0$ $\alpha > 0$	α is fixed	monotonically increase	$\gamma_0 = \frac{\alpha^2}{-4\mu_1}$	$a = \frac{\alpha}{2}$	Remain unchanged
	γ_0 is fixed	monotonically increase	$\alpha = 2\sqrt{-\gamma_0\mu_1}$	$a = \sqrt{-\gamma_0\mu_1}$	Monotonically decrease

to followers in system Laplacian matrix. The minimum nonzero eigenvalue $-\mu_1$ of submatrix represents algebraic connectivity of the subgraph. The bigger $-\mu_1$ is, the faster system maximal convergence rate is. Therefore, the minimum nonzero eigenvalue $-\mu_1$ can be increased (at least will not be decreased) by adding information links between spacecraft.

According to **Wely Theorem** [38], it can be proved that edge addition method can increase the minimum eigenvalue of submatrix. Information topology of spacecraft cluster system still needs to satisfy ***Assumption* 1** after adding edges.

Remark 5: There are two ways to add edges, one is to add bidirectional edges between followers, the other is to add directed edges from leaders to followers. It has been proved that the convergence rate of new system after adding edges is faster than original system[21]. Then for fixed contol gain coefficients α, γ_0, γ_1, adding bidirectional information interaction between followers or directed information interaction from leaders to followers can improve maximum convergence rate of cluster system.

Remark 6: It can be seen that increasing the weight of information links can also improve maximal convergence rate of large-scale cluster spacecraft system. The Laplacian matrix obtained by increasing the weight on an edge can also be seen as it is obtained from original Laplacian matrix plus a positive semi-definite matrix.

Remark 7: Usually, to keep the control force as small as possible, a smaller relative position feedback term γ_0 is selected. While according to Table 1, γ_0 cannot be too small, otherwise it will affect convergence rate of cluster system.

Although adding information links can increase the maximum convergence rate of cluster system, meanwhile it also increases the communication pressure of cluster system and wastes limited measurement, communication and computing resources on board. Information interaction may also be subject to external interference in complex space environment. We need to design appropriate information interaction topology to balance system convergence rate and communication pressure.

When information links between followers are directed, $\mathcal{G}_F$ is directed graph, then $\boldsymbol{L}_F$ has eigenvalues with non-zero imaginary parts. In general, it is difficult to obtain a regular result on convergence rate using eigenvalues of $\boldsymbol{\Gamma}$ under directed topology.

IV. COLLISION AVOIDANCE BASED ON INFORMATION TOPOLOGY DESIGN

For large-scale cluster flight missions, one of the problems to be considered is collision avoidance among cluster members. If two satellites appear in a certain position at the same time, a collision will occur and the satellites will be disabled. In order to ensure normal operation of the satellites, collision avoidance must be considered in coordinated orbit control of cluster satellites.

It indicates in [34] that the steady state of each follower is a convex combination of states of the leaders that can reach, and the combination coefficient is a quantity related to the system Laplace matrix. It can be concluded that the distribution of followers in the target region is determined by system information topology (including the weights that assigned to edges).

Note that the interactions between spacecraft need not be bidirectional in practice due to communication bandwidth or sensor capability. Constrained by inter-spacecraft distance and performance of sensors, only parts of followers can receive information from leaders directly.

In this section, approaches from graph theory to investigate influence of information topology on the distribution of followers are presented to provide a reference for collision avoidance.

A. THE CONSTRAINT OF LEADER REACHABLE SET ON STEADY STATE OF FOLLOWERS

According to the definition of reachable set [39], the follower i is reachable from leader $n+j$, then there exists a directed path from $n+j$ to i, namely, the motion of follower i will be affected directly or indirectly by leader $n+j$. If there doesn't exist directed path from $n+j$ to i, the motion of i will not be affected by leader $n+j$, thus the steady state of follower i is not related to $n+j$. If follower i is reachable from multiple leaders at the same time, the motion of i is affected by multiple leaders, and its stable state is correspondingly determined by the states of these leaders together.

Denote $\boldsymbol{C} = -\boldsymbol{L}_F^{-1}\boldsymbol{L}_{FL}$ as coefficient matrix of steady state of followers with respect to the state of leaders, where $0 \le c_{ij} \le 1, \sum_{j=1}^{m} c_{ij} = 1$. It reflects the relationship between system information topology and steady state of followers. If and only if follower i is reachable from multiple leaders including $n+j, 0 < c_{ij} < 1$. If follower i is only reachable from leader $n+j$, $c_{ij} = 1$. If follower i is not reachable from leader $n+j, c_{ij} = 0$.

Let $\boldsymbol{R}_j\ (j = 1, 2, \ldots m)$ is reachable set of leader $n+j$, $\boldsymbol{H}_j = \boldsymbol{R}_j \backslash \cup_{j\neq i} \boldsymbol{R}_i$ is a set of all followers which is only reachable from leader $n+j$. $\boldsymbol{Y}_j = \boldsymbol{F}\backslash\boldsymbol{R}_j$ represents unreachable set from leader $n+j$. Set $\boldsymbol{P}_j = \boldsymbol{R}_j\backslash\boldsymbol{H}_j$, and $\tilde{\boldsymbol{H}}_j = \boldsymbol{H}_j\backslash\{n+j\}$.

Then $\boldsymbol{L}_F$ *and* $\boldsymbol{L}_{FL}$ can be written in the following block matrix forms

$$\boldsymbol{L}_F = \begin{bmatrix} \boldsymbol{L}_{\tilde{H}_j} & 0 & 0 \\ \boldsymbol{L}_{P_j\tilde{H}} & \boldsymbol{L}_{P_j} & \boldsymbol{L}_{P_jY_j} \\ 0 & 0 & \boldsymbol{L}_{Y_j} \end{bmatrix}, \quad \boldsymbol{L}_{FL} = [\delta_1 \ldots \delta_m] \tag{21}$$

where $\boldsymbol{\delta}_j = \begin{bmatrix} \boldsymbol{L}_{H,n+j}^T \boldsymbol{L}_{P_j,n+j}^T\ 0 \end{bmatrix}^T$.

Theorem 4: Assume all leaders have converged to the steady states $\boldsymbol{r}_{n+1}^d, \boldsymbol{r}_{n+2}^d, \ldots, \boldsymbol{r}_{n+m}^d$ Then under the control of orbital containment control algorithm (2), all followers of cluster system (1) will asymptotically converge to the steady state $\boldsymbol{r}_i^d = \sum_{j=1}^{m} c_{ij}\boldsymbol{r}_{n+j}^d, i \in F$.

Proof: Since

$$\boldsymbol{L}_{\tilde{H}} 1_{\tilde{H}_j} + \boldsymbol{L}_{\tilde{H},n+j} = \boldsymbol{0} \tag{22}$$

we have

$$\boldsymbol{L}_{\tilde{H}_j}^{-1}\boldsymbol{L}_{\tilde{H},n+j} = -1_{\tilde{H}_j} \tag{23}$$

we can obtain that

$$\begin{aligned} -\boldsymbol{L}_F^{-1}\boldsymbol{\delta}_j &= -\begin{bmatrix} \boldsymbol{L}_{\tilde{H}_j}^{-1}\boldsymbol{L}_{\tilde{H}_j,n+j} \\ -\boldsymbol{L}_{P_j}^{-1}\boldsymbol{L}_{P_j\tilde{H}_j,n+j} + \boldsymbol{L}_{P_j}^{-1}\boldsymbol{L}_{P_j,n+j} \\ 0 \end{bmatrix} \\ &= \begin{bmatrix} 1_{\tilde{H}_j} \\ \boldsymbol{L}_{P_j}^{-1}\left(\boldsymbol{L}_{P_j\tilde{H}_j} 1_{\tilde{H}_j} + \boldsymbol{L}_{P_j,n+j}\right) \\ 0 \end{bmatrix} \end{aligned} \tag{24}$$

TABLE 2. Orbital elements of reference spacecraft.

a	e	i	Ω	ω	f
6998455	0.01	45	0	0	30

Further, each entry of $\boldsymbol{L}_{P_j}^{-1}\left(\boldsymbol{L}_{P_j\tilde{H}_j}\boldsymbol{1}_{\tilde{H}_j} + \boldsymbol{L}_{P_j,n+j}\right)$ is positive. Otherwise $\boldsymbol{L}_{P_j\tilde{H}_j}\boldsymbol{1}_{\tilde{H}_j} + \boldsymbol{L}_{P_j,n+j} = \boldsymbol{0}$, which means $\boldsymbol{P}_j$ doesn't have neighbors in $\boldsymbol{H}_j$, which contradicts to the definition of $\boldsymbol{P}_j$.

Now Theorem 4 has been proved.

B. THE CONSTRAINT OF GRAPH DIFFERENTIATION ON FOLLOWERS' DISTRIBUTION

In large-scale cluster flying spacecraft mission, each member obtains the information of neighbours by communication or relative state measurement. Due to the difference in the performance of relative measurement sensors and communication equipment, and relative distance between members, neighbour spacecraft sets which each cluster member can be sensitive to or communicate with are different. However, there may exist some commonalities among cluster members in information interaction, according to which cluster members can be divided into several subsets, and dynamic behaviour of cluster members belonging to the same subset may also have commonalities.

Although steady state of followers can be roughly estimated based on leader reachable set, collision avoidance design needs further analysis on state of followers. The steady state of followers can be described by using π^1 partition and π^2 partition of cluster information topology. These two graph theory tools can divide the cluster member spacecraft into several subsets, and the number of neighbours in other subsets of cluster members belonging to the same subset has a certain commonality, providing theoretical basis for system information topology of collision avoidance.

At first, we prove that the satellites in the same cell partition belonging to $\pi^1_{\{H_1,\ldots,H_m\}}$ partition have same steady state.

Theorem 5: For orbital containment control algorithm (2) of large-scale cluster system which satisfies $\boldsymbol{r}_F^d = -\boldsymbol{L}_F^{-1}\boldsymbol{L}_{FL}\boldsymbol{r}_L$ if system information topology $\mathcal{G}$ has a cell partition $\pi^1_{\{H_1,\ldots,H_m\}} = \{C_1, \ldots, C_k\}$, then all the followers that belong to the same cell $\boldsymbol{C}_i\ (i = 1, \ldots k)$ have the same steady state.

Proof: Suppose $\pi^1_{\{H_1,\ldots,H_m\}} = \{C_1, \ldots, C_k\}$ is a cell partition of $\mathcal{V}(\mathcal{G})$ with $\boldsymbol{C}_1 = \boldsymbol{H}_1, \ldots, \boldsymbol{C}_m = \boldsymbol{H}_m$, then according to the cell partition of $\mathcal{V}(\mathcal{G})$ by ordering the vertices appropriately, the graph Laplacian can be written in the following form

$$\mathcal{L} = \begin{bmatrix} \boldsymbol{L}_{C_1C_1} & \cdots & 0 & 0 & \cdots & 0 \\ \vdots & \ddots & \vdots & \vdots & \ddots & \vdots \\ 0 & \cdots & \boldsymbol{L}_{C_mC_m} & 0 & \cdots & 0 \\ \boldsymbol{L}_{C_{m+1}C_1} & \cdots & \boldsymbol{L}_{C_{m+1}C_m} & \boldsymbol{L}_{C_{m+1}C_{m+1}} & \cdots & \boldsymbol{L}_{C_{m+1}C_k} \\ \vdots & \ddots & \vdots & \vdots & \ddots & \vdots \\ \boldsymbol{L}_{C_kC_1} & \cdots & \boldsymbol{L}_{C_kC_m} & \boldsymbol{L}_{C_kC_{m+1}} & \cdots & \boldsymbol{L}_{C_kC_k} \end{bmatrix}$$

TABLE 3. Initial state of followers.

Index of followers	Initial position (m)	Initial velocity (m/s)
1	$\boldsymbol{r}_1(0)=[469,-485,200]^{\mathrm{T}}$	$\dot{\boldsymbol{r}}_1(0)=[0.06,0,-0.01]^{\mathrm{T}}$
2	$\boldsymbol{r}_2(0)=[469,485,100]^{\mathrm{T}}$	$\dot{\boldsymbol{r}}_2(0)=[0.06,-0.03,0.01]^{\mathrm{T}}$
3	$\boldsymbol{r}_3(0)=[-300,519,-100]^{\mathrm{T}}$	$\dot{\boldsymbol{r}}_3(0)=[-0.03,0.07,0.02]^{\mathrm{T}}$
4	$\boldsymbol{r}_4(0)=[-300,-519,-200]^{\mathrm{T}}$	$\dot{\boldsymbol{r}}_4(0)=[0.02,0.03,-0.02]^{\mathrm{T}}$
5	$\boldsymbol{r}_5(0)=[104,-590,0]^{\mathrm{T}}$	$\dot{\boldsymbol{r}}_5(0)=[0.05,-0.06,0.02]^{\mathrm{T}}$
6	$\boldsymbol{r}_6(0)=[104,590,0]^{\mathrm{T}}$	$\dot{\boldsymbol{r}}_6(0)=[-0.06,0.02,0]^{\mathrm{T}}$
7	$\boldsymbol{r}_7(0)=[-563,205,-100]^{\mathrm{T}}$	$\dot{\boldsymbol{r}}_7(0)=[0.06,0.03,-0.04]^{\mathrm{T}}$
8	$\boldsymbol{r}_8(0)=[-563,-205,-200]^{\mathrm{T}}$	$\dot{\boldsymbol{r}}_8(0)=[0.03,0.01,0.07]^{\mathrm{T}}$
9	$\boldsymbol{r}_9(0)=[400,-585,100]^{\mathrm{T}}$	$\dot{\boldsymbol{r}}_9(0)=[0.02,0.03,-0.04]^{\mathrm{T}}$
10	$\boldsymbol{r}_{10}(0)=[400,585,200]^{\mathrm{T}}$	$\dot{\boldsymbol{r}}_{10}(0)=[0.02,0.03,-0.01]^{\mathrm{T}}$
11	$\boldsymbol{r}_{11}(0)=[-469,380,-200]^{\mathrm{T}}$	$\dot{\boldsymbol{r}}_{11}(0)=[0.04,-0.02,0.01]^{\mathrm{T}}$
12	$\boldsymbol{r}_{12}(0)=[-469,-380,100]^{\mathrm{T}}$	$\dot{\boldsymbol{r}}_{12}(0)=[0.07,0.03,-0.01]^{\mathrm{T}}$
13	$\boldsymbol{r}_{13}(0)=[300,519,100]^{\mathrm{T}}$	$\dot{\boldsymbol{r}}_{13}(0)=[-0.04,0.05,0.03]^{\mathrm{T}}$
14	$\boldsymbol{r}_{14}(0)=[300,-519,200]^{\mathrm{T}}$	$\dot{\boldsymbol{r}}_{14}(0)=[0.02,-0.03,0.01]^{\mathrm{T}}$
15	$\boldsymbol{r}_{15}(0)=[-104,590,100]^{\mathrm{T}}$	$\dot{\boldsymbol{r}}_{15}(0)=[0.05,0.04,-0.02]^{\mathrm{T}}$
16	$\boldsymbol{r}_{16}(0)=[-104,-590,200]^{\mathrm{T}}$	$\dot{\boldsymbol{r}}_{16}(0)=[0.01,-0.02,0.06]^{\mathrm{T}}$
17	$\boldsymbol{r}_{17}(0)=[563,205,200]^{\mathrm{T}}$	$\dot{\boldsymbol{r}}_{17}(0)=[0.03,-0.07,0.04]^{\mathrm{T}}$
18	$\boldsymbol{r}_{18}(0)=[563,-205,100]^{\mathrm{T}}$	$\dot{\boldsymbol{r}}_{18}(0)=[0.04,-0.01,0.05]^{\mathrm{T}}$
19	$\boldsymbol{r}_{19}(0)=[-400,-480,200]^{\mathrm{T}}$	$\dot{\boldsymbol{r}}_{19}(0)=[0.01,-0.03,0.04]^{\mathrm{T}}$
20	$\boldsymbol{r}_{20}(0)=[-400,480,100]^{\mathrm{T}}$	$\dot{\boldsymbol{r}}_{20}(0)=[0.02,0.02,-0.03]^{\mathrm{T}}$

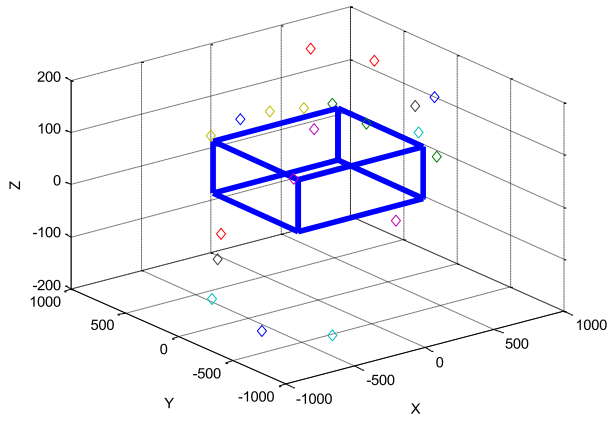

FIGURE 1. Initial position of followers and target area.

The block matrix at the lower left corner and the lower right corner are denoted by $\boldsymbol{A},\boldsymbol{B}$, respectively. Since $\boldsymbol{L}\boldsymbol{r}_F^d=0,\boldsymbol{A}\boldsymbol{r}_H^d+\boldsymbol{B}\boldsymbol{r}_{\bar{F}}^d=0$ is obtained. Then by Lemma 2 in [34], $\boldsymbol{r}_{\bar{F}}^d=-\boldsymbol{B}^{-1}\boldsymbol{A}\boldsymbol{r}_H^d$. Assuming that each vertex in C_i has s_{ij} number of neighbors in $\boldsymbol{C}_j$ $(i,j=1,\ldots k,i\neq k)$, then, according to the definition of π^1 partition each row sum of the submatrix $\boldsymbol{L}_{C_iC_j}$ $(i,j=1,\ldots,k,i\neq j)$ equals s_{ij}. Combining with Corollary 1 in [34], it is given that

$$\boldsymbol{A}\boldsymbol{r}_H^d=\begin{bmatrix}-s_{m+1,1}1_{rm+1}\\ \vdots\\ -s_{k,1}1_{rk}\end{bmatrix}\boldsymbol{r}_{n+1}^d+\cdots+\begin{bmatrix}-s_{m+1,m}1_{rm+1}\\ \vdots\\ -s_{k,m}1_{rk}\end{bmatrix}\boldsymbol{r}_{n+m}^d$$

where $\boldsymbol{r}_i$ is the cardinality of i $\boldsymbol{C}_i$ $(i{=}m{+}1,\ldots,k)$

It follows that

$$\boldsymbol{r}_{\bar{F}}^d=\boldsymbol{B}^{-1}\begin{bmatrix}s_{m+1,1}1_{rm+1}\\ \vdots\\ s_{k,1}1_{rk}\end{bmatrix}\boldsymbol{r}_{n+1}^d+\cdots+\boldsymbol{B}^{-1}\begin{bmatrix}s_{m+1,m}1_{rm+1}\\ \vdots\\ s_{k,m}1_{rk}\end{bmatrix}\boldsymbol{r}_{n+m}^d$$

By using Lemma 3 in [34], it can be concluded that all the followers that belong to the same cell $Ci(i{=}1,\ldots,k)$ have the same steady state.

Now Theorem 5 has been proved.

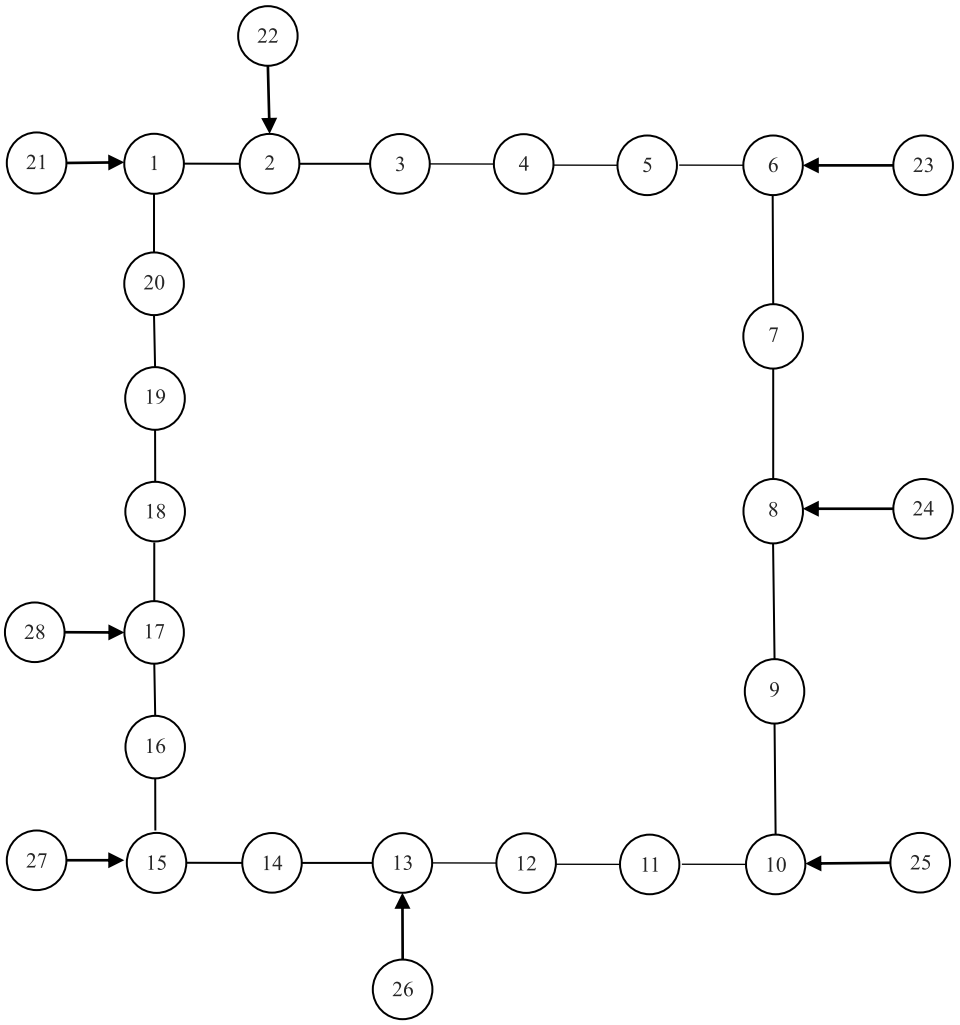

FIGURE 2. System information topology.

Then, another cell partition, $\pi^2_{\{H_1,\ldots,H_m\}}$ partition is provided to prove that satellites in the same cell partition belonging to $\pi^2_{\{H_1,\ldots,H_m\}}$ partition have the same steady state.

Theorem 6: For containment control algorithms satisfying $\boldsymbol{r}_F^d = -\boldsymbol{L}_F^{-1}\boldsymbol{L}_{FL}\boldsymbol{r}_L$, if the system information topology $\mathcal{G}$ has a cell partition $\pi^2_{\{H_1,\ldots,H_m\}} = \{C_1,\ldots,C_k\}$ with $\boldsymbol{C}_i \subseteq \boldsymbol{H}_j$ or $\boldsymbol{C}_i \subseteq \boldsymbol{F}, i = 1,\ldots,k, j = 1,\ldots,m$, then all the followers that belonging to the same cell $\boldsymbol{C}_i$ $(i = 1,\ldots k)$ have the same steady state.

Proof [34]: Construct the deduced unweighted graph $\bar{\mathcal{G}}^2$ of $\mathcal{G}$ as follows: use a follower $\bar{i}$ to represent cell $\boldsymbol{C}_i$ draw an edge from $\bar{j}$ to $\bar{i}$ is a neighbor cell of $\boldsymbol{C}_i$. Then, $\bar{\mathcal{G}}^2$ has m reaches according to Assumptions 1. Let $\bar{L}^2$ be the Laplacian matrix of the deduced graph $\bar{\mathcal{G}}^2$, it can be derived that $\bar{\boldsymbol{L}}^2\bar{\boldsymbol{r}}_F = \boldsymbol{0}$ with $\bar{\boldsymbol{r}}_i = \boldsymbol{r}^d_{n+j}$ if $\boldsymbol{C}_i \subseteq \boldsymbol{H}_j$ has unique solution.

$$\boldsymbol{L}_F = \begin{bmatrix}
3 & -1 & 0 & 0 & 0 & 0 & 0 & 0 & 0 & 0 & 0 & 0 & 0 & 0 & 0 & 0 & 0 & 0 & 0 & -1 \\
-1 & 3 & -1 & 0 & 0 & 0 & 0 & 0 & 0 & 0 & 0 & 0 & 0 & 0 & 0 & 0 & 0 & 0 & 0 & 0 \\
0 & -1 & 2 & -1 & 0 & 0 & 0 & 0 & 0 & 0 & 0 & 0 & 0 & 0 & 0 & 0 & 0 & 0 & 0 & 0 \\
0 & 0 & -1 & 2 & -1 & 0 & 0 & 0 & 0 & 0 & 0 & 0 & 0 & 0 & 0 & 0 & 0 & 0 & 0 & 0 \\
0 & 0 & 0 & -1 & 2 & -1 & 0 & 0 & 0 & 0 & 0 & 0 & 0 & 0 & 0 & 0 & 0 & 0 & 0 & 0 \\
0 & 0 & 0 & 0 & -1 & 3 & -1 & 0 & 0 & 0 & 0 & 0 & 0 & 0 & 0 & 0 & 0 & 0 & 0 & 0 \\
0 & 0 & 0 & 0 & 0 & -1 & 2 & -1 & 0 & 0 & 0 & 0 & 0 & 0 & 0 & 0 & 0 & 0 & 0 & 0 \\
0 & 0 & 0 & 0 & 0 & 0 & -1 & 3 & -1 & 0 & 0 & 0 & 0 & 0 & 0 & 0 & 0 & 0 & 0 & 0 \\
0 & 0 & 0 & 0 & 0 & 0 & 0 & -1 & 2 & -1 & 0 & 0 & 0 & 0 & 0 & 0 & 0 & 0 & 0 & 0 \\
0 & 0 & 0 & 0 & 0 & 0 & 0 & 0 & -1 & 3 & -1 & 0 & 0 & 0 & 0 & 0 & 0 & 0 & 0 & 0 \\
0 & 0 & 0 & 0 & 0 & 0 & 0 & 0 & 0 & -1 & 2 & -1 & 0 & 0 & 0 & 0 & 0 & 0 & 0 & 0 \\
0 & 0 & 0 & 0 & 0 & 0 & 0 & 0 & 0 & 0 & -1 & 3 & -1 & 0 & 0 & 0 & 0 & 0 & 0 & 0 \\
0 & 0 & 0 & 0 & 0 & 0 & 0 & 0 & 0 & 0 & 0 & -1 & 2 & -1 & 0 & 0 & 0 & 0 & 0 & 0 \\
0 & 0 & 0 & 0 & 0 & 0 & 0 & 0 & 0 & 0 & 0 & 0 & -1 & 3 & -1 & 0 & 0 & 0 & 0 & 0 \\
0 & 0 & 0 & 0 & 0 & 0 & 0 & 0 & 0 & 0 & 0 & 0 & 0 & -1 & 2 & -1 & 0 & 0 & 0 & 0 \\
0 & 0 & 0 & 0 & 0 & 0 & 0 & 0 & 0 & 0 & 0 & 0 & 0 & 0 & -1 & 3 & -1 & 0 & 0 & 0 \\
0 & 0 & 0 & 0 & 0 & 0 & 0 & 0 & 0 & 0 & 0 & 0 & 0 & 0 & 0 & -1 & 2 & -1 & 0 & 0 \\
0 & 0 & 0 & 0 & 0 & 0 & 0 & 0 & 0 & 0 & 0 & 0 & 0 & 0 & 0 & 0 & -1 & 2 & -1 & 0 \\
0 & 0 & 0 & 0 & 0 & 0 & 0 & 0 & 0 & 0 & 0 & 0 & 0 & 0 & 0 & 0 & 0 & -1 & 2 & -1 \\
-1 & 0 & 0 & 0 & 0 & 0 & 0 & 0 & 0 & 0 & 0 & 0 & 0 & 0 & 0 & 0 & 0 & 0 & -1 & 2
\end{bmatrix}, \quad \boldsymbol{L}_{FL} = \begin{bmatrix}
-1 & 0 & 0 & 0 & 0 & 0 & 0 & 0 \\
0 & -1 & 0 & 0 & 0 & 0 & 0 & 0 \\
0 & 0 & 0 & 0 & 0 & 0 & 0 & 0 \\
0 & 0 & 0 & 0 & 0 & 0 & 0 & 0 \\
0 & 0 & 0 & 0 & 0 & 0 & 0 & 0 \\
0 & 0 & -1 & 0 & 0 & 0 & 0 & 0 \\
0 & 0 & 0 & 0 & 0 & 0 & 0 & 0 \\
0 & 0 & 0 & -1 & 0 & 0 & 0 & 0 \\
0 & 0 & 0 & 0 & 0 & 0 & 0 & 0 \\
0 & 0 & 0 & 0 & -1 & 0 & 0 & 0 \\
0 & 0 & 0 & 0 & 0 & 0 & 0 & 0 \\
0 & 0 & 0 & 0 & 0 & 0 & 0 & 0 \\
0 & 0 & 0 & 0 & 0 & -1 & 0 & 0 \\
0 & 0 & 0 & 0 & 0 & 0 & 0 & 0 \\
0 & 0 & 0 & 0 & 0 & 0 & -1 & 0 \\
0 & 0 & 0 & 0 & 0 & 0 & 0 & 0 \\
0 & 0 & 0 & 0 & 0 & 0 & 0 & -1 \\
0 & 0 & 0 & 0 & 0 & 0 & 0 & 0 \\
0 & 0 & 0 & 0 & 0 & 0 & 0 & 0 \\
0 & 0 & 0 & 0 & 0 & 0 & 0 & 0
\end{bmatrix}$$

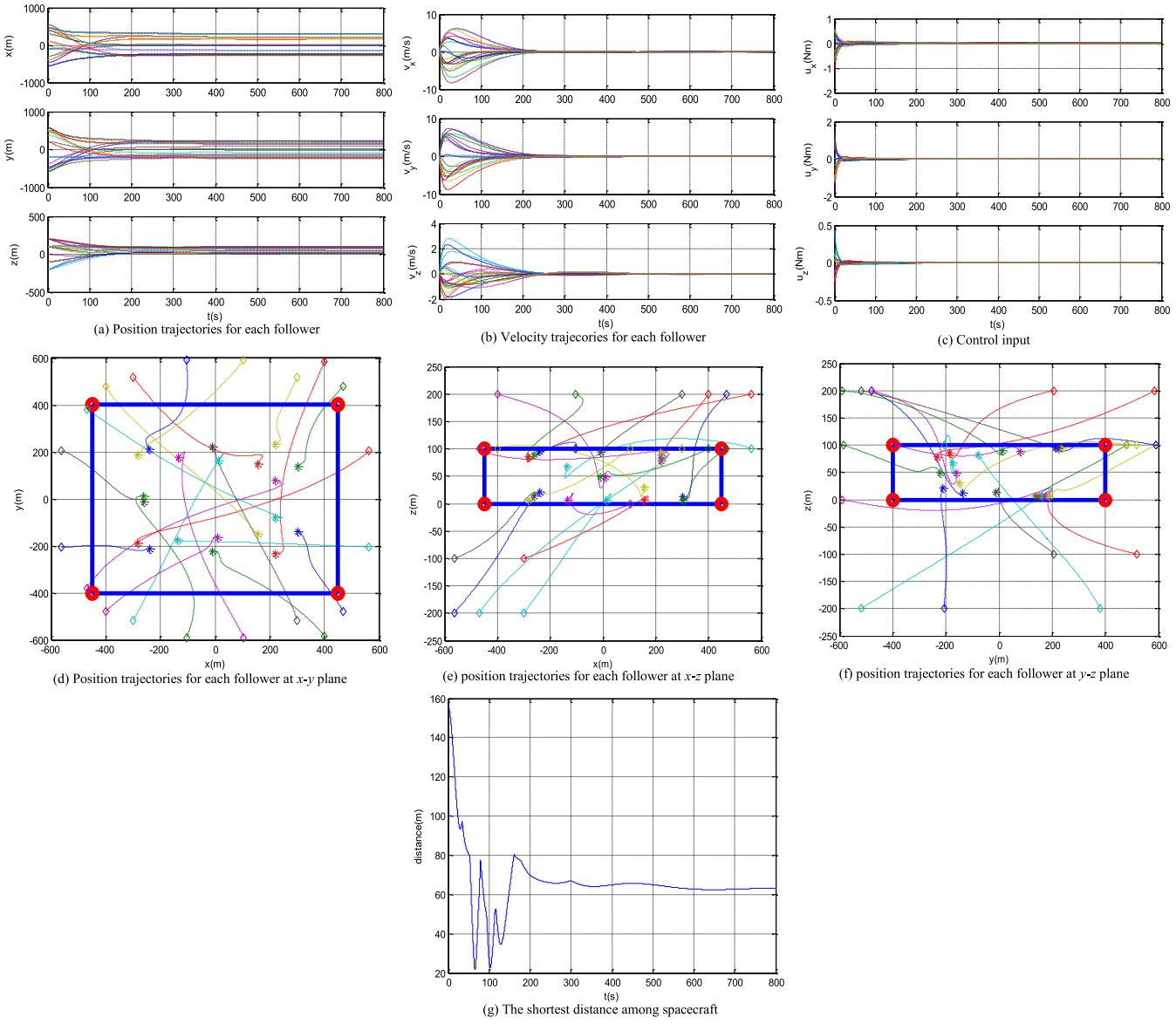

FIGURE 3. Simulation results for $\gamma_0 = \frac{1}{1600}$, $\gamma_1 = 0.0438$.

Finally, it can be verified that $\boldsymbol{r}^d_{FC_i} = \bar{r}_i \mathbf{1}_{C_i}$ is the solution of $\bar{\boldsymbol{L}}\bar{r}^d_F = \mathbf{0}$.

Now Theorem 6 has been proved.

V. SIMULATION RESULTS

In this section, simulations for a multiple leader-follower spacecraft cluster are presented to illustrate effectiveness of the proposed control approach and information topology design. In most Earth-orbiting cluster flying spacecraft, J_2 disturbance is the dominant perturbation force by two orders of magnitude [22], [24], and thus in the simulations only the effects of $\boldsymbol{J}_2$ disturbance are considered, whereas the effect of other disturbance forces result from atmospheric drag, solar radiation, and third-body effects are not taken into consideration here.

The $\boldsymbol{J}_2$ disturbance force expressed as

$$f_{J_2} = \frac{3}{2}\mu_\oplus J_2 R_\oplus^2 \left[5\frac{r_x r_z^2}{r^7} - \frac{r_x}{r^5}, 5\frac{r_y r_z^2}{r^7} - \frac{r_y}{r^5}, 5\frac{r_z^3}{r^7} - 3\frac{r_z}{r^5}\right]^T$$

where r_x, r_y, r_z are the position vector components of followers. $\boldsymbol{J}_2 = 0.0010826$, $R_\oplus = 6371km$ is the mean equatorial radius of Earth. In addition, 10^{-6} order white noise disturbance is considered in the simulation.

In this scenario, the proposed containment control algorithm (2) is tested in an orbit motion simulation of a cluster of 28 spacecraft. The 20 spacecraft, denoted by $F = \{1, 2, \ldots, 20\}$, should be controlled into a cuboid area formed by 8 vertices which is denoted by $L = \{21, 22, \ldots, 28\}$.

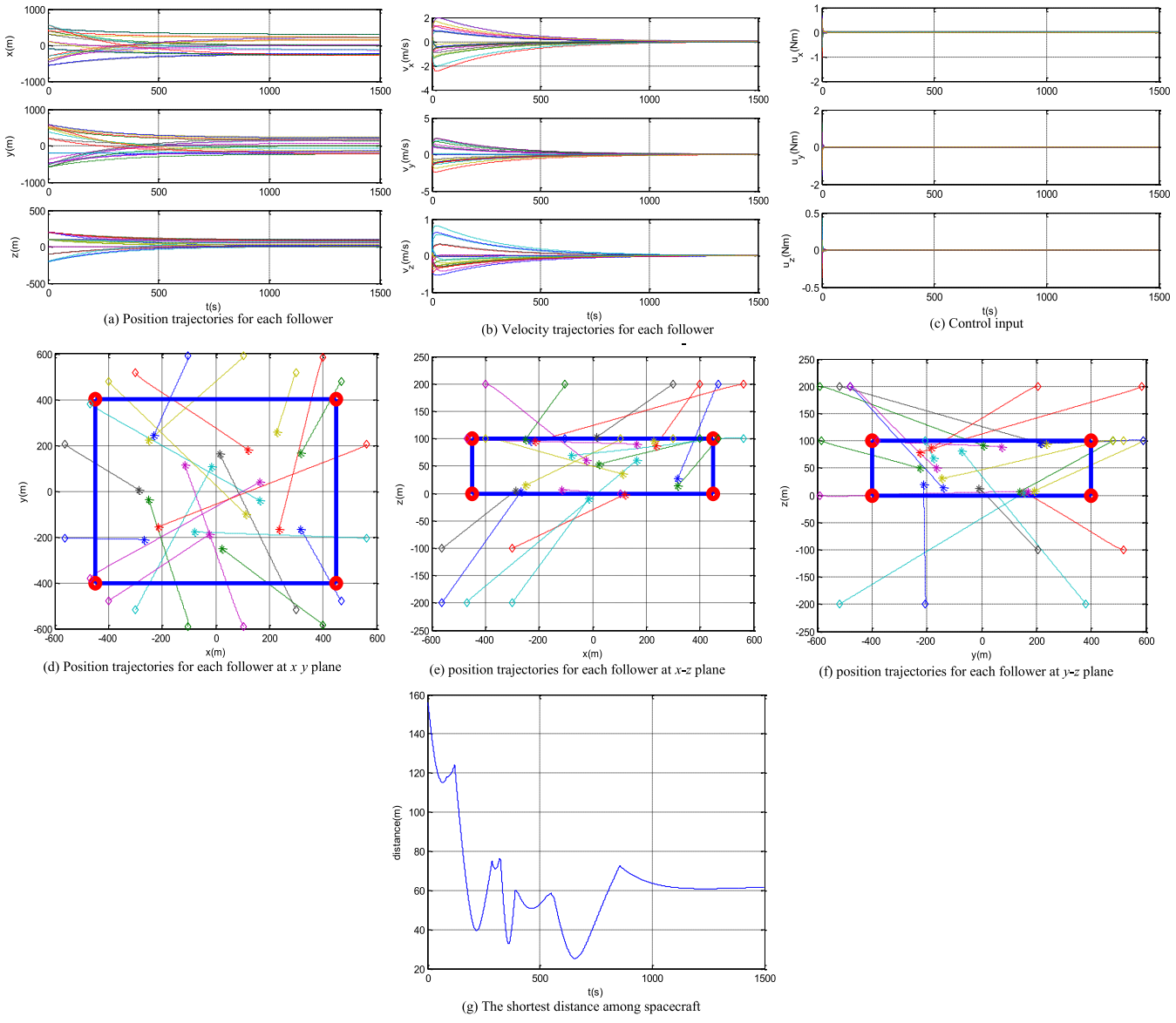

FIGURE 4. Simulation results for $\gamma_0 = \frac{1}{1600}$, $\gamma_1 = 0.2$.

The position of leaders in reference coordinate frame respectively are (unit:m)

$$\boldsymbol{r}_{21} = [430, -360, 0]^{\mathrm{T}} \quad \boldsymbol{r}_{25} = [430, -360, 200]^{\mathrm{T}}$$
$$\boldsymbol{r}_{22} = [430, 360, 0]^{\mathrm{T}} \quad \boldsymbol{r}_{26} = [430, 360, 200]^{\mathrm{T}}$$
$$\boldsymbol{r}_{23} = [-430, 360, 0]^{\mathrm{T}} \quad \boldsymbol{r}_{27} = [-430, 360, 200]^{\mathrm{T}}$$
$$\boldsymbol{r}_{24} = [-430, -360, 0]^{\mathrm{T}} \quad \boldsymbol{r}_{28} = [-430, -360, 200]^{\mathrm{T}}$$

Relative position of each follower to the target area at initial moment is shown in Fig. 1. We can find that all the followers are outside the convex hull formed by leaders initially.

Suppose that system information topology is shown as Fig. 2, then Laplacian matrices respectively are $\boldsymbol{L}_F, \boldsymbol{L}_{FL}$, as shown at the bottom of the 11th page.

The initial state of followers in reference orbit coordinate frame are respectively shown in Table 3.

It has been calculated that eigenvalues of $\boldsymbol{L}_F$ are about 4.5221, 4.4631, 4.4203, 4.1649, 4.0333, 3.6328, 3.5697, 3.2651, 2.9336, 2.4152, 2.3667, 1.7002, 1.6311, 1.2005, 1.1821, 0.7862, 0.6865, 0.4017, 0.3480, 0.2771.

A. THE INFLUENCE OF INFORMATION TOPOLOGY DESIGN ON CONTROL PERFORMANCE

1) THE INFLUENCE OF COEFFICIENT ON CONVERGENCE RATE

To control all cluster members into the convex full formed by leaders with a fast convergence rate using controller (2), control gain coefficient needs to meet certain conditions. The purpose of the simulation in this section is to verify the constraint conditions of **Theorem 3** and convergence rate on control gain coefficient. The effects of control gain

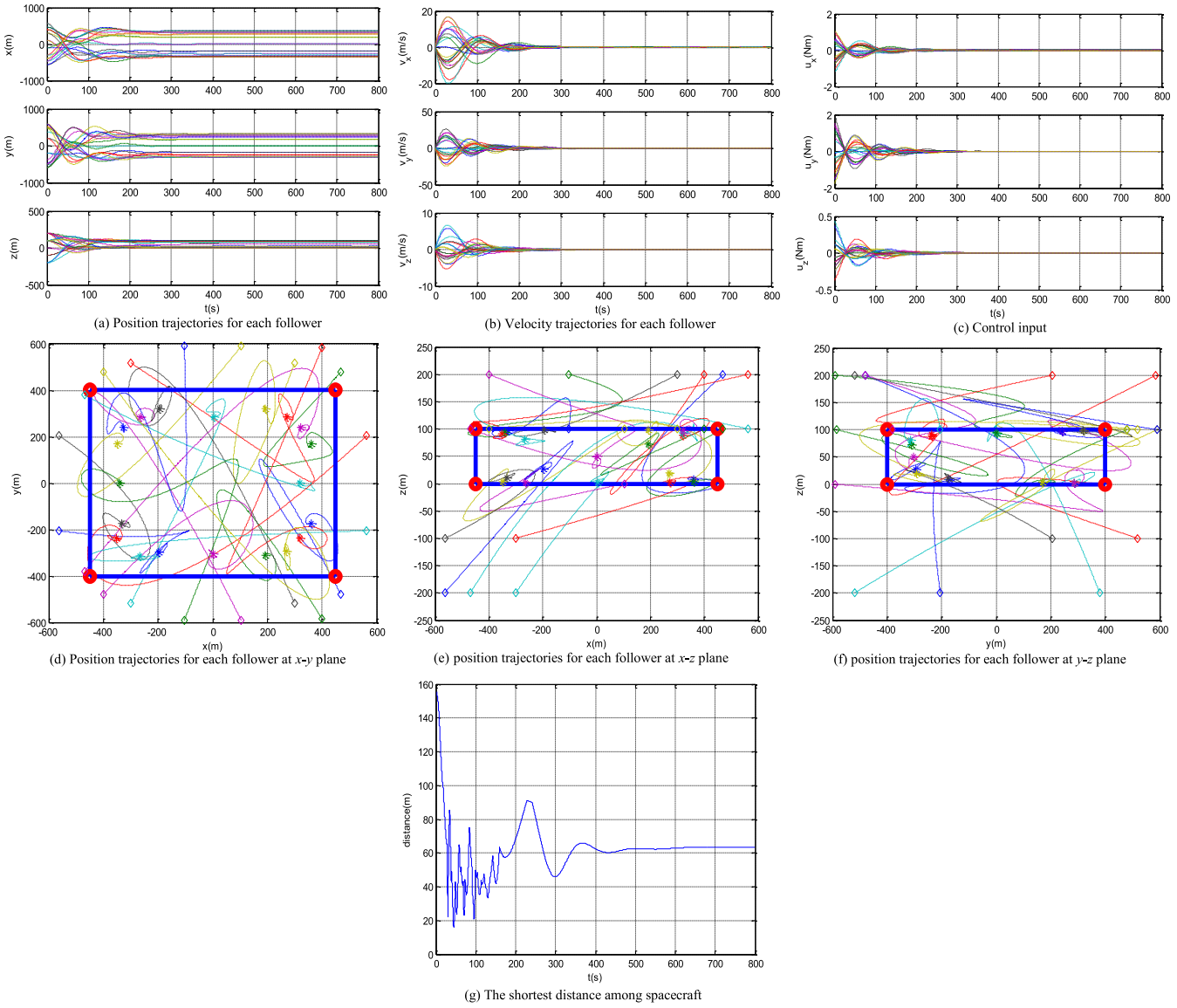

(a) Position trajectories for each follower
(b) Velocity trajectories for each follower
(c) Control input
(d) Position trajectories for each follower at x-y plane
(e) position trajectories for each follower at x-z plane
(f) position trajectories for each follower at y-z plane
(g) The shortest distance among spacecraft

FIGURE 5. Simulation results for $\gamma_0 = \frac{1}{1600}$, $\alpha = 0.0263$.

coefficient on control performance are explained in detail through simulation results.

2) CONTROLLER WITHOUT ABSOLUTE VELOCITY CONTROL TERM

When $\alpha = 0$, $\gamma_0 > 0$, $\gamma_1 > 0$, controller (2) does not contain absolute velocity control term of member spacecraft relative to reference spacecraft. The influence of control gain coefficient on convergence and convergence rate is analysed.

According to calculation of control gain coefficient expression in Section III, If $\gamma_0 = \frac{1}{1600}$, when $\gamma_1 = 0.0438$ cluster system converges to convex full with the maximal convergence rate. The simulation results in Fig. 3 show that all followers will converge into the target area formed by the leaders within 200s, and relative velocity converge to 0 within 400s. In the control process, followers will not collide with each other.

As a comparison, $\gamma_0 = \frac{1}{1600}$, $\gamma_1 = 0.2$ are selected, and simulation results are shown as Fig. 4. The simulation results show that all followers will converge into the target area formed by the leaders. But the convergence time be increased to 900s, relative velocity converge to 0 within 1100s. In the control process, followers will not collide with each other.

Simulation results show that these two control gain coefficients can control these 20 followers into target area, but a maximal convergence rate will be obtained at $\gamma_0 = \frac{1}{1600}$, $\gamma_1 = 0.0438$.

3) CONTROLLER WITHOUT RELATIVE VELOCITY CONTROL TERM

The initial conditions of simulation remain the same. When $\gamma_1 = 0$, $\gamma_0 > 0$, $\alpha > 0$, controller (2) does not

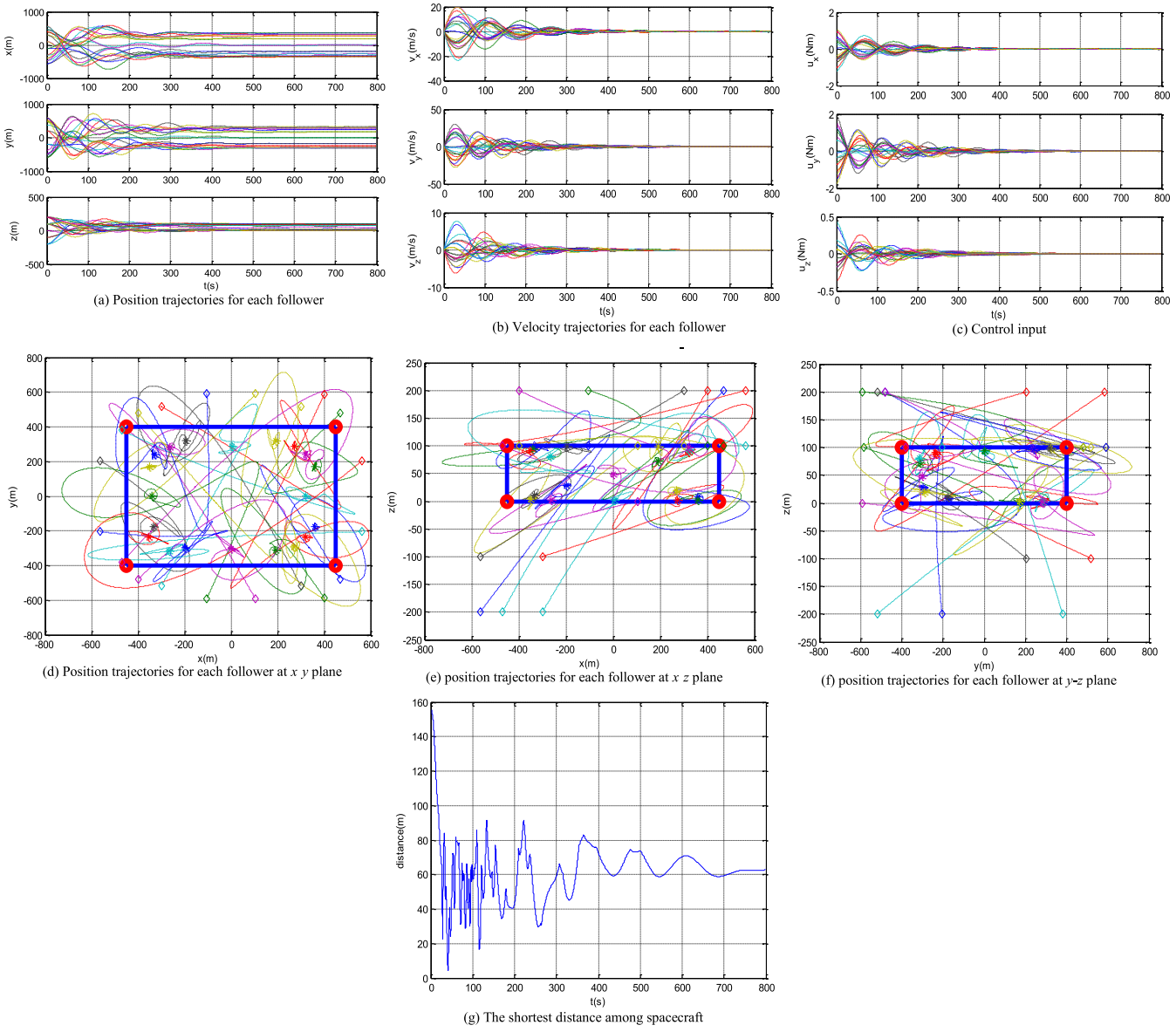

FIGURE 6. **Simulation results for $\gamma_0 = \frac{1}{1600}$, $\alpha = 0.015$.**

contain relative velocity control term of member spacecraft relative to reference spacecraft. The influence of control gain coefficient on convergence and convergence rate are analysed.

If $\gamma_0 = \frac{1}{1600}$, when $\alpha = 0.0263$ cluster system converges to the target area formed by leaders with the maximal convergence rate. The simulation results in Fig. 5 show that all followers will converge into the target area formed by the leaders within 200s, relative velocity converge to 0 within 250s. In the control process, followers will not collide with each other.

As a comparison, $\gamma_0 = \frac{1}{1600}$, $\alpha = 0.015$ are selected, and simulation results are shown as Fig. 6. The simulation results show that all followers will converge into the target area formed by the leaders, but all followers will converge into the target area formed by the leaders within 300s, relative velocity converge to 0 within 400s. And the nearest distance of followers will near 0m, collision may collide in the control process.

Simulation results show that these two control gain coefficients can control these 20 followers into target area, but a maximal convergence rate will be obtained at $\gamma_0 = \frac{1}{1600}$, $\alpha = 0.0263$.

4) THE INFLUENCE OF INFORMATION TOPOLOGY ON CONVERGENCE RATE

In this section, the influence of edge add method on convergence rate is verified.

Edges from leaders to followers (21, 20), (22, 3), (23, 5), (24, 7), (25, 9), (26, 12), (27, 14), (28, 18) are added on the

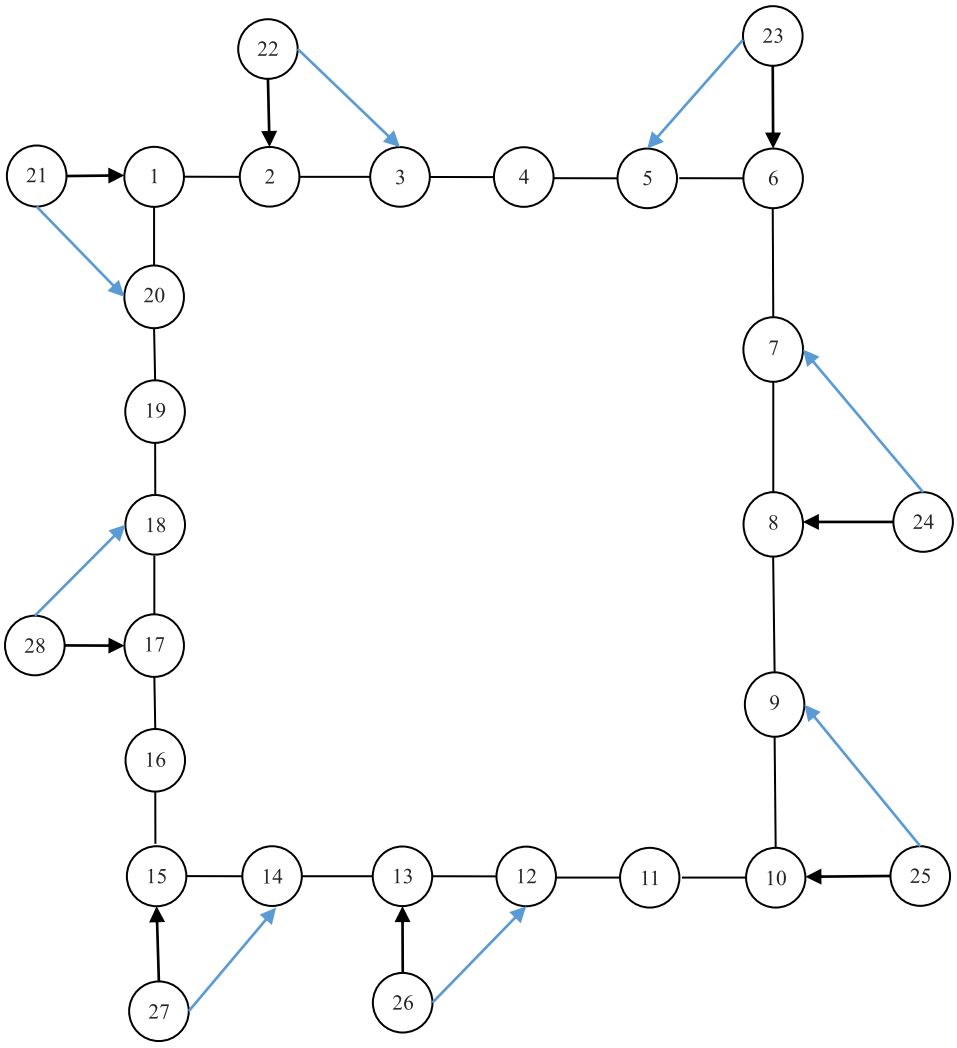

FIGURE 7. Information topology after adding edges.

basis of original information topology (Fig. 2), then new system information topology is shown as Fig. 7.

It has been calculated that eigenvalues of $\boldsymbol{L}_F$ are about 4.8866, 4.7746, 4.7746, 4.4689, 4.4498, 4, 4, 3.5847, 3.2607, 2.8141, 2.8141, 2.3393, 2.0863, 1.6396, 1.6396, 1.2855, 0.9736, 0.7717, 0.7717, 0.6646. Obviously, all the eigenvalues of $\boldsymbol{L}_F$ are increased after adding edges.

Laplacian matrices respectively are $\boldsymbol{L}_F$, $\boldsymbol{L}_{FL}$, as shown at the bottom of the page.

Control gain coefficient $\alpha = 0$, $\gamma_1 = 0.0438$ are selected, then the followers will be driven into the target area formed by leaders with maximal convergence rate when $\gamma_0 = 5.9418 \times 10^{-4}$. Simulation results in Fig. 8 show that all followers will be driven into the target area formed

$$\boldsymbol{L}_F = \begin{bmatrix}
3 & -1 & 0 & 0 & 0 & 0 & 0 & 0 & 0 & 0 & 0 & 0 & 0 & 0 & 0 & 0 & 0 & 0 & 0 & 0 & -1 \\
-1 & 3 & -1 & 0 & 0 & 0 & 0 & 0 & 0 & 0 & 0 & 0 & 0 & 0 & 0 & 0 & 0 & 0 & 0 & 0 & 0 \\
0 & -1 & 3 & -1 & 0 & 0 & 0 & 0 & 0 & 0 & 0 & 0 & 0 & 0 & 0 & 0 & 0 & 0 & 0 & 0 & 0 \\
0 & 0 & -1 & 2 & -1 & 0 & 0 & 0 & 0 & 0 & 0 & 0 & 0 & 0 & 0 & 0 & 0 & 0 & 0 & 0 & 0 \\
0 & 0 & 0 & -1 & 3 & -1 & 0 & 0 & 0 & 0 & 0 & 0 & 0 & 0 & 0 & 0 & 0 & 0 & 0 & 0 & 0 \\
0 & 0 & 0 & 0 & -1 & 3 & -1 & 0 & 0 & 0 & 0 & 0 & 0 & 0 & 0 & 0 & 0 & 0 & 0 & 0 & 0 \\
0 & 0 & 0 & 0 & 0 & -1 & 3 & -1 & 0 & 0 & 0 & 0 & 0 & 0 & 0 & 0 & 0 & 0 & 0 & 0 & 0 \\
0 & 0 & 0 & 0 & 0 & 0 & -1 & 3 & -1 & 0 & 0 & 0 & 0 & 0 & 0 & 0 & 0 & 0 & 0 & 0 & 0 \\
0 & 0 & 0 & 0 & 0 & 0 & 0 & -1 & 3 & -1 & 0 & 0 & 0 & 0 & 0 & 0 & 0 & 0 & 0 & 0 & 0 \\
0 & 0 & 0 & 0 & 0 & 0 & 0 & 0 & -1 & 3 & -1 & 0 & 0 & 0 & 0 & 0 & 0 & 0 & 0 & 0 & 0 \\
0 & 0 & 0 & 0 & 0 & 0 & 0 & 0 & 0 & -1 & 2 & -1 & 0 & 0 & 0 & 0 & 0 & 0 & 0 & 0 & 0 \\
0 & 0 & 0 & 0 & 0 & 0 & 0 & 0 & 0 & 0 & -1 & 3 & -1 & 0 & 0 & 0 & 0 & 0 & 0 & 0 & 0 \\
0 & 0 & 0 & 0 & 0 & 0 & 0 & 0 & 0 & 0 & 0 & -1 & 3 & -1 & 0 & 0 & 0 & 0 & 0 & 0 & 0 \\
0 & 0 & 0 & 0 & 0 & 0 & 0 & 0 & 0 & 0 & 0 & 0 & -1 & 3 & -1 & 0 & 0 & 0 & 0 & 0 & 0 \\
0 & 0 & 0 & 0 & 0 & 0 & 0 & 0 & 0 & 0 & 0 & 0 & 0 & -1 & 2 & -1 & 0 & 0 & 0 & 0 & 0 \\
0 & 0 & 0 & 0 & 0 & 0 & 0 & 0 & 0 & 0 & 0 & 0 & 0 & 0 & -1 & 3 & -1 & 0 & 0 & 0 & 0 \\
0 & 0 & 0 & 0 & 0 & 0 & 0 & 0 & 0 & 0 & 0 & 0 & 0 & 0 & 0 & -1 & 3 & -1 & 0 & 0 & 0 \\
0 & 0 & 0 & 0 & 0 & 0 & 0 & 0 & 0 & 0 & 0 & 0 & 0 & 0 & 0 & 0 & -1 & 3 & -1 & 0 & 0 \\
0 & 0 & 0 & 0 & 0 & 0 & 0 & 0 & 0 & 0 & 0 & 0 & 0 & 0 & 0 & 0 & 0 & -1 & 2 & -1 & 0 \\
-1 & 0 & 0 & 0 & 0 & 0 & 0 & 0 & 0 & 0 & 0 & 0 & 0 & 0 & 0 & 0 & 0 & 0 & -1 & 3 & -1 \\
0 & 0 & 0 & 0 & 0 & 0 & 0 & 0 & 0 & 0 & 0 & 0 & 0 & 0 & 0 & 0 & 0 & 0 & 0 & -1 & 3
\end{bmatrix}, \quad \boldsymbol{L}_{FL} = \begin{bmatrix}
-1 & 0 & 0 & 0 & 0 & 0 & 0 & 0 \\
0 & -1 & 0 & 0 & 0 & 0 & 0 & 0 \\
0 & -1 & 0 & 0 & 0 & 0 & 0 & 0 \\
0 & 0 & 0 & 0 & 0 & 0 & 0 & 0 \\
0 & 0 & -1 & 0 & 0 & 0 & 0 & 0 \\
0 & 0 & -1 & 0 & 0 & 0 & 0 & 0 \\
0 & 0 & 0 & -1 & 0 & 0 & 0 & 0 \\
0 & 0 & 0 & -1 & 0 & 0 & 0 & 0 \\
0 & 0 & 0 & 0 & -1 & 0 & 0 & 0 \\
0 & 0 & 0 & 0 & -1 & 0 & 0 & 0 \\
0 & 0 & 0 & 0 & 0 & 0 & 0 & 0 \\
0 & 0 & 0 & 0 & 0 & -1 & 0 & 0 \\
0 & 0 & 0 & 0 & 0 & -1 & 0 & 0 \\
0 & 0 & 0 & 0 & 0 & 0 & -1 & 0 \\
0 & 0 & 0 & 0 & 0 & 0 & -1 & 0 \\
0 & 0 & 0 & 0 & 0 & 0 & 0 & 0 \\
0 & 0 & 0 & 0 & 0 & 0 & 0 & -1 \\
0 & 0 & 0 & 0 & 0 & 0 & 0 & -1 \\
0 & 0 & 0 & 0 & 0 & 0 & 0 & 0 \\
-1 & 0 & 0 & 0 & 0 & 0 & 0 & 0
\end{bmatrix}$$

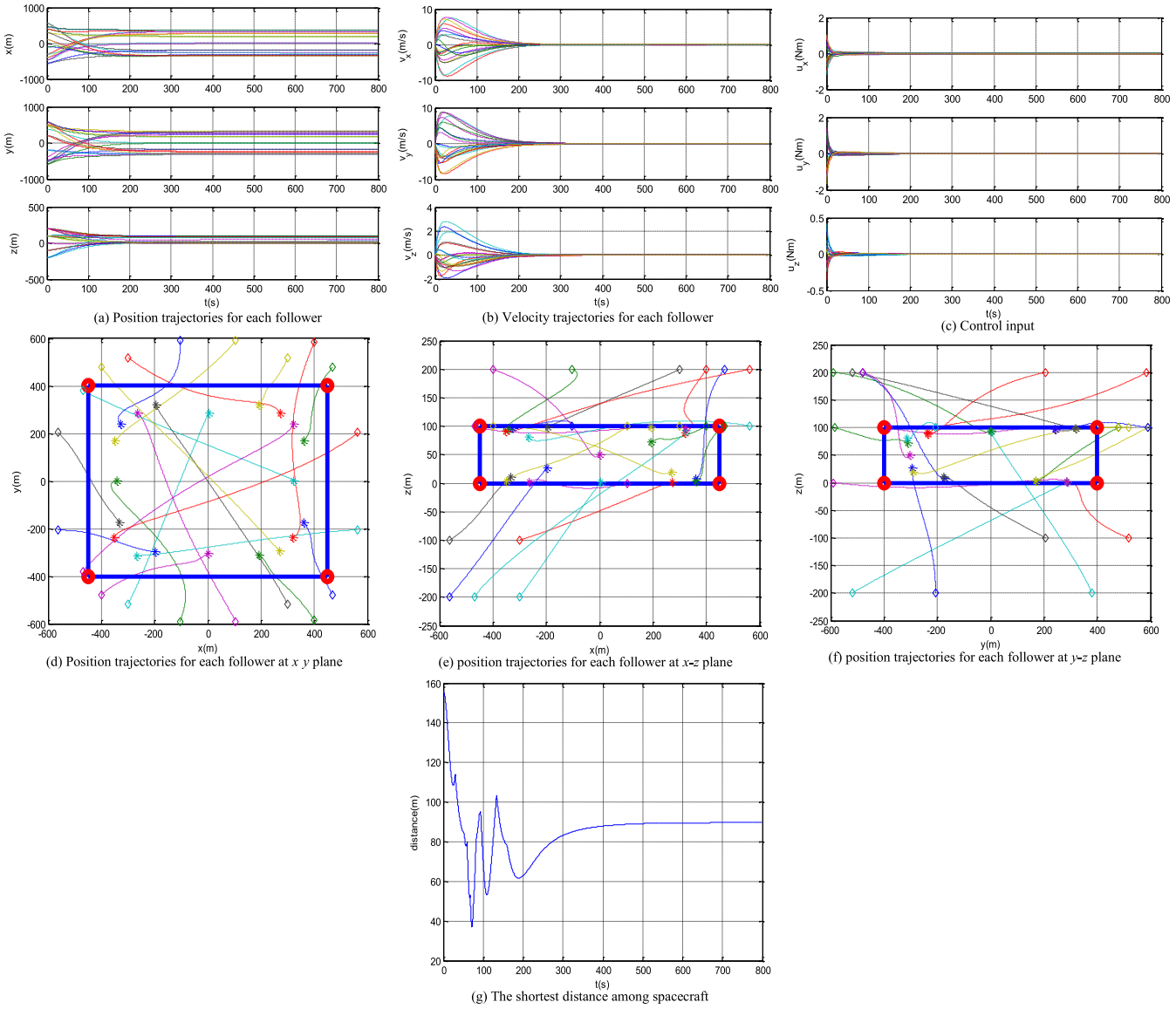

(a) Position trajectories for each follower
(b) Velocity trajectories for each follower
(c) Control input
(d) Position trajectories for each follower at x y plane
(e) position trajectories for each follower at x-z plane
(f) position trajectories for each follower at y-z plane
(g) The shortest distance among spacecraft

FIGURE 8. Simulation results for $\gamma_0 = 5.9418 \times 10^{-4}$, $\gamma_1 = 0.0438$.

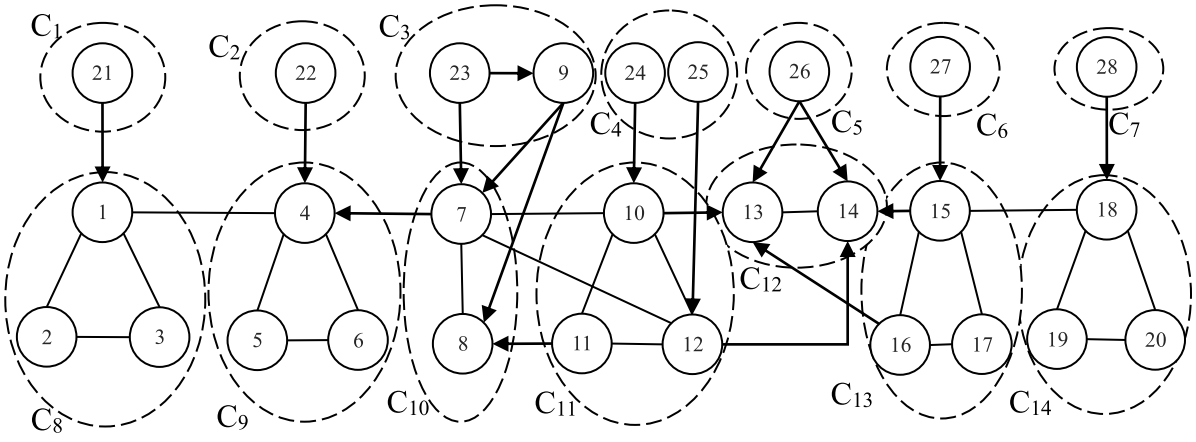

FIGURE 9. Information topology.

by the leaders, and the convergence time will be decreased to 120s, relative velocity converges to 0 within 300s. In the control process, followers will not collide with each other. Comparing the motion trajectories of each follower in Fig. 3, it can be seen that the maximal convergence rate of system will be increased after adding information links.

B. THE INFLUENCE OF INFORMATION TOPOLOGY DESIGN ON DISTRIBUTION OF FOLLOWERS

1) THE CASE OF COLLISIONS

Using Orbital containment control algorithm (2), control gain coefficients are chosen as $\alpha = 0.05,\ \gamma_0 = 1/1600,\ \gamma_1 = 0$. Safe collision avoidance distance is $10m$.

Suppose that system information topology is shown as Fig. 9, then Laplacian matrices respectively are $\boldsymbol{L}_F, \boldsymbol{L}_{FL}$. The relationship matrix between the follower's stable state and the leader's state is $\boldsymbol{C} = -\boldsymbol{L}_F^{-1}\boldsymbol{L}_{FL}$, as shown at the bottom of the page. Simulation results are shown as Fig. 10.

Simulation results show that the shortest distance between followers in the final stage is close to 0, thus collisions are easy to occur. This case is due to the fact that information topology shown in Figure 9 contains π^2 differentiation. Such as spacecraft 1,2,3 belong to C_8 cell, spacecraft 4,5,6 belong to C_9 cell, spacecraft 7,8 belong to C_{10} cell, spacecraft 15,16,17 belong to C_{13} cell, spacecraft and 18,19,20 belong to C_{14} cell. According to Theorem 6, the spacecraft belonging to the same cells will converge to the same location in the target area and collide with each other, respectively. In addition, spacecraft 9 only receives information from virtual leader 23, its motion is influenced by leader 23 and perturbation, thus spacecraft 9 will converge into the target area and the position of it will near leader 23.

According to Theorem 4, 5 and 6, and simulation results of Fig. 9 and Fig. 10, if followers have the completely consistent state coefficients, they will converge to the same location in the control process.

In order to avoid collisions among cluster members, the original information topology needs to be modified appropriately so that each spacecraft can make reasonable use of the received information.

$$\boldsymbol{L}_F = \begin{bmatrix}
4 & -1 & -1 & -1 & 0 & 0 & 0 & 0 & 0 & 0 & 0 & 0 & 0 & 0 & 0 & 0 & 0 & 0 & 0 & 0 \\
-1 & 2 & -1 & 0 & 0 & 0 & 0 & 0 & 0 & 0 & 0 & 0 & 0 & 0 & 0 & 0 & 0 & 0 & 0 & 0 \\
-1 & -1 & 2 & 0 & 0 & 0 & 0 & 0 & 0 & 0 & 0 & 0 & 0 & 0 & 0 & 0 & 0 & 0 & 0 & 0 \\
-1 & 0 & 0 & 5 & -1 & -1 & -1 & 0 & 0 & 0 & 0 & 0 & 0 & 0 & 0 & 0 & 0 & 0 & 0 & 0 \\
0 & 0 & 0 & -1 & 2 & -1 & 0 & 0 & 0 & 0 & 0 & 0 & 0 & 0 & 0 & 0 & 0 & 0 & 0 & 0 \\
0 & 0 & 0 & -1 & -1 & 2 & 0 & 0 & 0 & 0 & 0 & 0 & 0 & 0 & 0 & 0 & 0 & 0 & 0 & 0 \\
0 & 0 & 0 & 0 & 0 & 0 & 5 & -1 & -1 & -1 & 0 & -1 & 0 & 0 & 0 & 0 & 0 & 0 & 0 & 0 \\
0 & 0 & 0 & 0 & 0 & 0 & -1 & 3 & -1 & 0 & -1 & 0 & 0 & 0 & 0 & 0 & 0 & 0 & 0 & 0 \\
0 & 0 & 0 & 0 & 0 & 0 & 0 & 0 & 1 & 0 & 0 & 0 & 0 & 0 & 0 & 0 & 0 & 0 & 0 & 0 \\
0 & 0 & 0 & 0 & 0 & 0 & -1 & 0 & 0 & 4 & -1 & -1 & 0 & 0 & 0 & 0 & 0 & 0 & 0 & 0 \\
0 & 0 & 0 & 0 & 0 & 0 & 0 & 0 & 0 & -1 & 2 & -1 & 0 & 0 & 0 & 0 & 0 & 0 & 0 & 0 \\
0 & 0 & 0 & 0 & 0 & 0 & -1 & 0 & 0 & -1 & -1 & 4 & 0 & 0 & 0 & 0 & 0 & 0 & 0 & 0 \\
0 & 0 & 0 & 0 & 0 & 0 & 0 & 0 & 0 & -1 & 0 & 0 & 4 & -1 & 0 & -1 & 0 & 0 & 0 & 0 \\
0 & 0 & 0 & 0 & 0 & 0 & 0 & 0 & 0 & 0 & 0 & -1 & -1 & 4 & -1 & 0 & 0 & 0 & 0 & 0 \\
0 & 0 & 0 & 0 & 0 & 0 & 0 & 0 & 0 & 0 & 0 & 0 & 0 & 4 & -1 & -1 & -1 & 0 & 0 & 0 \\
0 & 0 & 0 & 0 & 0 & 0 & 0 & 0 & 0 & 0 & 0 & 0 & 0 & -1 & 2 & -1 & 0 & 0 & 0 & 0 \\
0 & 0 & 0 & 0 & 0 & 0 & 0 & 0 & 0 & 0 & 0 & 0 & 0 & -1 & -1 & 2 & 0 & 0 & 0 & 0 \\
0 & 0 & 0 & 0 & 0 & 0 & 0 & 0 & 0 & 0 & 0 & 0 & 0 & -1 & 0 & 0 & 4 & -1 & -1 & 0 \\
0 & 0 & 0 & 0 & 0 & 0 & 0 & 0 & 0 & 0 & 0 & 0 & 0 & 0 & 0 & 0 & -1 & 2 & -1 & 0 \\
0 & 0 & 0 & 0 & 0 & 0 & 0 & 0 & 0 & 0 & 0 & 0 & 0 & 0 & 0 & 0 & -1 & -1 & 2 & 0 \\
0 & 0 & 0 & 0 & 0 & 0 & 0 & 0 & 0 & 0 & 0 & 0 & 0 & 0 & 0 & 0 & 0 & 0 & 0 & 0
\end{bmatrix}, \quad \boldsymbol{L}_{FL} = \begin{bmatrix}
-1 & 0 & 0 & 0 & 0 & 0 & 0 & 0 \\
0 & 0 & 0 & 0 & 0 & 0 & 0 & 0 \\
0 & 0 & 0 & 0 & 0 & 0 & 0 & 0 \\
0 & -1 & 0 & 0 & 0 & 0 & 0 & 0 \\
0 & 0 & 0 & 0 & 0 & 0 & 0 & 0 \\
0 & 0 & 0 & 0 & 0 & 0 & 0 & 0 \\
0 & 0 & -1 & 0 & 0 & 0 & 0 & 0 \\
0 & 0 & 0 & 0 & 0 & 0 & 0 & 0 \\
0 & 0 & -1 & 0 & 0 & 0 & 0 & 0 \\
0 & 0 & 0 & -1 & 0 & 0 & 0 & 0 \\
0 & 0 & 0 & 0 & 0 & 0 & 0 & 0 \\
0 & 0 & 0 & 0 & -1 & 0 & 0 & 0 \\
0 & 0 & 0 & 0 & 0 & -1 & 0 & 0 \\
0 & 0 & 0 & 0 & 0 & -1 & 0 & 0 \\
0 & 0 & 0 & 0 & 0 & 0 & 0 & 0 \\
0 & 0 & 0 & 0 & 0 & 0 & -1 & 0 \\
0 & 0 & 0 & 0 & 0 & 0 & 0 & 0 \\
0 & 0 & 0 & 0 & 0 & 0 & 0 & -1 \\
0 & 0 & 0 & 0 & 0 & 0 & 0 & 0 \\
0 & 0 & 0 & 0 & 0 & 0 & 0 & 0
\end{bmatrix}$$

$$\boldsymbol{C} = -\boldsymbol{L}_F^{-1}\boldsymbol{L}_{FL} = \begin{bmatrix}
0.6 & 0.2 & 0.134 & 0.033 & 0.033 & 0 & 0 & 0 \\
0.6 & 0.2 & 0.134 & 0.033 & 0.033 & 0 & 0 & 0 \\
0.6 & 0.2 & 0.134 & 0.033 & 0.033 & 0 & 0 & 0 \\
0.2 & 0.4 & 0.266 & 0.067 & 0.067 & 0 & 0 & 0 \\
0.2 & 0.4 & 0.266 & 0.067 & 0.067 & 0 & 0 & 0 \\
0.2 & 0.4 & 0.266 & 0.067 & 0.067 & 0 & 0 & 0 \\
0 & 0 & 0.666 & 0.167 & 0.167 & 0 & 0 & 0 \\
0 & 0 & 0.666 & 0.167 & 0.167 & 0 & 0 & 0 \\
0 & 01 & 0 & 0 & 0 & 0 & 0 & \\
0 & 0 & 0.33 & 0.43 & 0.24 & 0 & 0 & 0 \\
0 & 0 & 0.34 & 0.33 & 0.33 & 0 & 0 & 0 \\
0 & 0 & 0.33 & 0.24 & 0.43 & 0 & 0 & 0 \\
0 & 0 & 0.11 & 0.13 & 0.10 & 0.33 & 0.22 & 0.11 \\
0 & 0 & 0.11 & 0.10 & 0.13 & 0.33 & 0.22 & 0.11 \\
0 & 0 & 0 & 0 & 0 & 0 & 0.67 & 0.33 \\
0 & 0 & 0 & 0 & 0 & 0 & 0.67 & 0.33 \\
0 & 0 & 0 & 0 & 0 & 0 & 0.67 & 0.33 \\
0 & 0 & 0 & 0 & 0 & 0 & 0.33 & 0.67 \\
0 & 0 & 0 & 0 & 0 & 0 & 0.33 & 0.67 \\
0 & 0 & 0 & 0 & 0 & 0 & 0.33 & 0.67
\end{bmatrix}$$

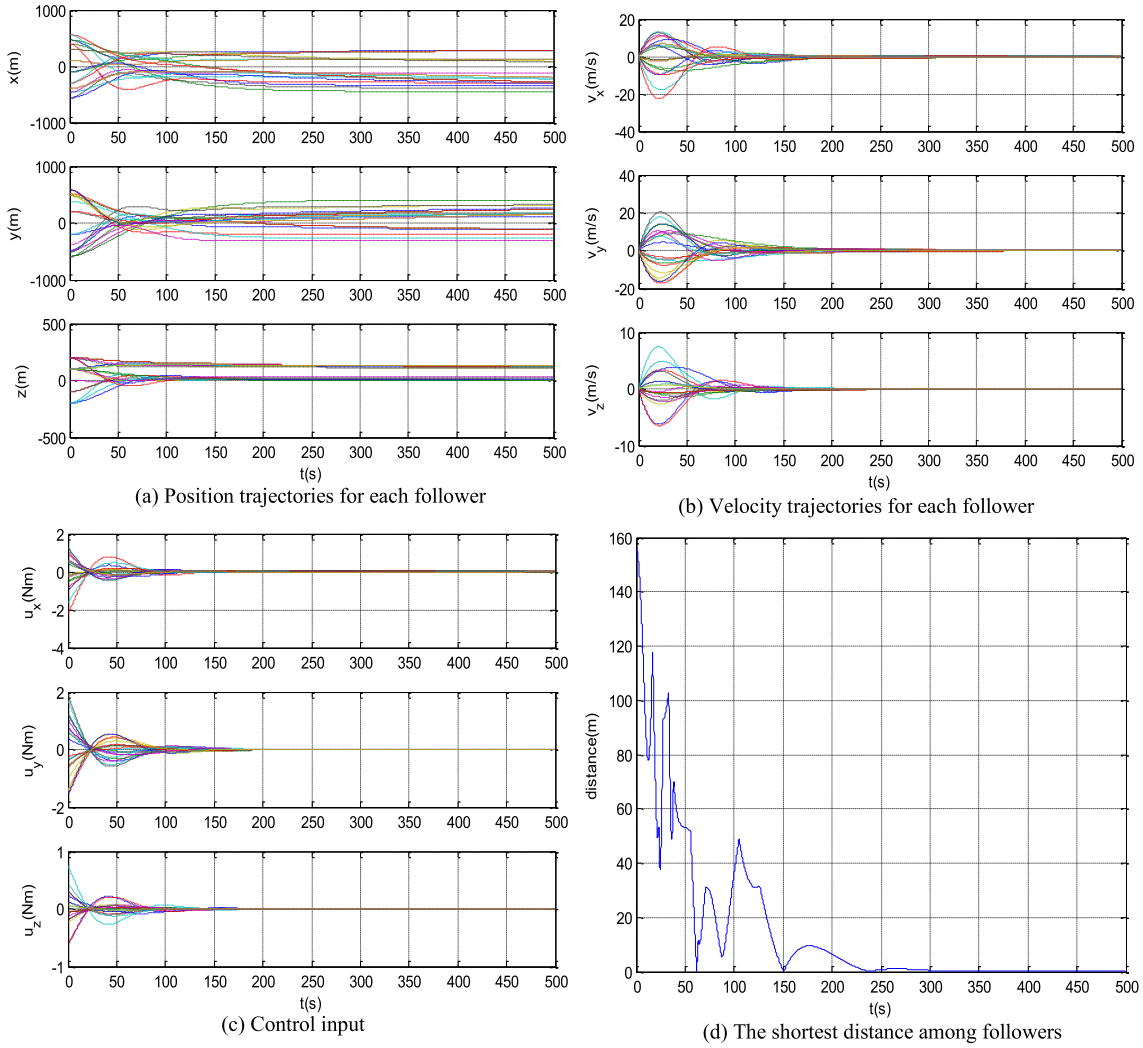

FIGURE 10. Simulation results with Fig.9 as information topology.

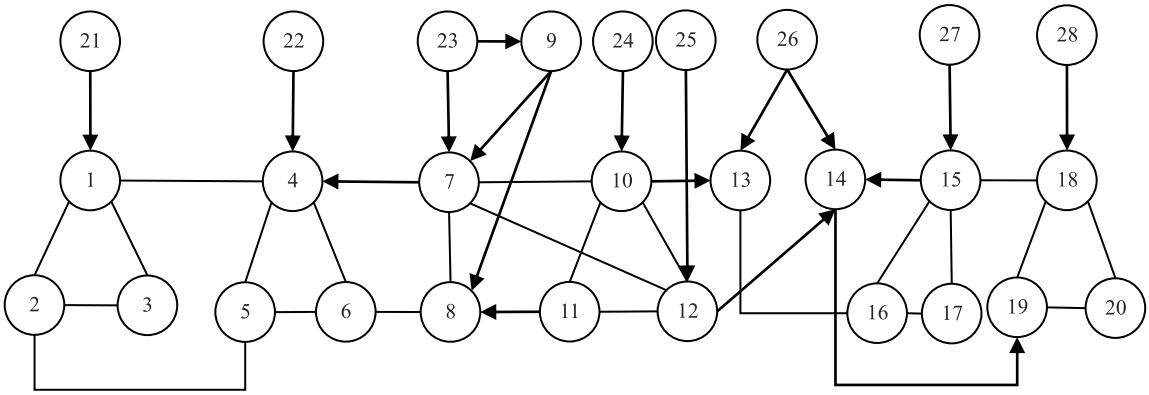

FIGURE 11. Information topology.

2) THE CASE OF COLLISION AVOIDANCE

The modified information topology is shown in Figure 11. Control gain coefficients are the same as the previous subsection. The modified information topology no longer contains π^2 differentiation, which is verified by simulation. Collisions will not collide for nano-satellite cluster under modified information topology. Simulation results show that the shortest distance among followers is around 11m.

Laplacian matrices respectively are $\boldsymbol{L}_F$, $\boldsymbol{L}_{FL}$, as shown at the bottom of the page.

The relationship matrix between the follower's stable state and the leader's state is $\boldsymbol{C} = -\boldsymbol{L}_F^{-1}\boldsymbol{L}_{FL}$, as shown at the bottom of the page.

C. THE PERFORMANCE OF POTENTION FUNCTION METHOD

In Ref.[28], [40], the artificial potential energy method is used to avoid collisions between spacecraft. Taking [40] for example, coordinated orbital control algorithm based on variable weight coefficient method is designed as follows.

$$\begin{aligned} u_{x_i} &= -3\omega^2 x_i - 2\omega\dot{y}_i - \alpha\dot{x}_i - \beta\left(x_i - x_i^d\right) \\ &\quad - \sum_{j\in N_i} a_{ij}\varpi_{ij}[(x_i - x_j) - (x_i^d - x_j^d)] \\ u_{y_i} &= 2\omega\dot{x}_i - \alpha\dot{y}_i - \beta\left(y_i - y_i^d\right) \\ &\quad - \sum_{j\in N_i} a_{ij}\varpi_{ij}[(y_i - y_j) - (y_i^d - y_j^d)] \\ u_{z_i} &= \omega^2 z_i - \alpha\dot{z}_i - \beta\left(z_i - z_i^d\right) \\ &\quad - \sum_{j\in N_i} a_{ij}\varpi_{ij}[(z_i - z_j) - (z_i^d - z_j^d)] \end{aligned} \tag{25}$$

where $\alpha > 0, \beta > 0, a_{ij} > 0$ represent adjacent coefficients between spacecraft. x_i^d, y_i^d, z_i^d respectively represent the desired state of spacecraft i in three-axis. Construct variable weight coefficient sum ϖ_{ij} as follows

$$\varpi_{ij} = \frac{\left|\left\|(r_i - r_j) - \left(r_i^d - r_j^d\right)\right\| - 2\left(\delta + \left\|r_i^d - r_j^d\right\|\right)\right|}{\left[\left\|(r_i - r_j) - \left(r_i^d - r_j^d\right)\right\| - \left(\delta + \left\|r_i^d - r_j^d\right\|\right)\right]^2} \tag{26}$$

where $\delta > 0$ is safe collision avoidance distance.

$$\boldsymbol{L}_F = \begin{bmatrix}
0 & 0 & 0 & 0 & 0 & 0 & 0 & 0 & 0 & 0 & 0 & 0 & 0 & 0 \\
0 & 0 & 0 & 0 & 0 & 0 & 0 & 0 & 0 & 0 & 0 & 0 & 0 & 0 \\
0 & 0 & 0 & 0 & 0 & 0 & 0 & 0 & 0 & 0 & 0 & 0 & 0 & 0 \\
0 & 0 & 0 & 0 & 0 & 0 & 0 & 0 & 0 & 0 & 0 & 0 & 0 & 0 \\
0 & 0 & 0 & 0 & 0 & 0 & 0 & 0 & 0 & 0 & 0 & 0 & 0 & 0 \\
-1 & 0 & 0 & 0 & 0 & 0 & 0 & 0 & 0 & 0 & 0 & 0 & 0 & 0 \\
-1 & -1 & -1 & 0 & -1 & 0 & 0 & 0 & 0 & 0 & 0 & 0 & 0 & 0 \\
4 & -1 & 0 & -1 & 0 & 0 & 0 & 0 & 0 & 0 & 0 & 0 & 0 & 0 \\
0 & 1 & 0 & 0 & 0 & 0 & 0 & 0 & 0 & 0 & 0 & 0 & 0 & 0 \\
0 & 0 & 4 & -1 & -1 & 0 & 0 & 0 & 0 & 0 & 0 & 0 & 0 & 0 \\
0 & 0 & -1 & 2 & -1 & 0 & 0 & 0 & 0 & 0 & 0 & 0 & 0 & 0 \\
0 & 0 & -1 & -1 & 4 & 0 & 0 & 0 & 0 & 0 & 0 & 0 & 0 & 0 \\
0 & 0 & -1 & 0 & 0 & 3 & 0 & 0 & -1 & 0 & 0 & 0 & 0 & 0 \\
0 & 0 & 0 & 0 & -1 & 0 & 3 & -1 & 0 & 0 & 0 & 0 & 0 & 0 \\
0 & 0 & 0 & 0 & 0 & 0 & 0 & 4 & -1 & -1 & -1 & 0 & 0 & 0 \\
0 & 0 & 0 & 0 & 0 & -1 & 0 & -1 & 3 & -1 & 0 & 0 & 0 & 0 \\
0 & 0 & 0 & 0 & 0 & 0 & 0 & -1 & -1 & 2 & 0 & 0 & 0 & 0 \\
0 & 0 & 0 & 0 & 0 & 0 & 0 & -1 & 0 & 0 & 4 & -1 & -1 & 0 \\
0 & 0 & 0 & 0 & 0 & 0 & -1 & 0 & 0 & 0 & -1 & 3 & -1 & 0 \\
0 & 0 & 0 & 0 & 0 & 0 & 0 & 0 & 0 & 0 & -1 & -1 & 2 & 0
\end{bmatrix}, \boldsymbol{L}_{FL} = \begin{bmatrix}
-1 & 0 & 0 & 0 & 0 & 0 & 0 & 0 \\
0 & 0 & 0 & 0 & 0 & 0 & 0 & 0 \\
0 & 0 & 0 & 0 & 0 & 0 & 0 & 0 \\
0 & -1 & 0 & 0 & 0 & 0 & 0 & 0 \\
0 & 0 & 0 & 0 & 0 & 0 & 0 & 0 \\
0 & 0 & 0 & 0 & 0 & 0 & 0 & 0 \\
0 & 0 & -1 & 0 & 0 & 0 & 0 & 0 \\
0 & 0 & 0 & 0 & 0 & 0 & 0 & 0 \\
0 & 0 & -1 & 0 & 0 & 0 & 0 & 0 \\
0 & 0 & 0 & -1 & 0 & 0 & 0 & 0 \\
0 & 0 & 0 & 0 & 0 & 0 & 0 & 0 \\
0 & 0 & 0 & 0 & -1 & 0 & 0 & 0 \\
0 & 0 & 0 & 0 & 0 & -1 & 0 & 0 \\
0 & 0 & 0 & 0 & 0 & -1 & 0 & 0 \\
0 & 0 & 0 & 0 & 0 & 0 & -1 & 0 \\
0 & 0 & 0 & 0 & 0 & 0 & 0 & 0 \\
0 & 0 & 0 & 0 & 0 & 0 & 0 & 0 \\
0 & 0 & 0 & 0 & 0 & 0 & 0 & -1 \\
0 & 0 & 0 & 0 & 0 & 0 & 0 & 0 \\
0 & 0 & 0 & 0 & 0 & 0 & 0 & 0
\end{bmatrix}$$

$$\boldsymbol{C} = -\boldsymbol{L}_F^{-1}\boldsymbol{L}_{FL} = \begin{bmatrix}
0.516 & 0.188 & 0.198 & 0.049 & 0.049 & 0 & 0 & 0 \\
0.412 & 0.215 & 0.249 & 0.062 & 0.062 & 0 & 0 & 0 \\
0.464 & 0.201 & 0.223 & 0.056 & 0.056 & 0 & 0 & 0 \\
0.190 & 0.335 & 0.317 & 0.079 & 0.079 & 0 & 0 & 0 \\
0.254 & 0.256 & 0.328 & 0.081 & 0.081 & 0 & 0 & 0 \\
0.163 & 0.217 & 0.414 & 0.103 & 0.103 & 0 & 0 & 0 \\
0.011 & 0.015 & 0.650 & 0.162 & 0.162 & 0 & 0 & 0 \\
0.045 & 0.060 & 0.597 & 0.149 & 0.149 & 0 & 0 & 0 \\
0 & 0 & 1 & 0 & 0 & 0 & 0 & 0 \\
0.006 & 0.007 & 0.325 & 0.431 & 0.231 & 0 & 0 & 0 \\
0.006 & 0.007 & 0.325 & 0.331 & 0.331 & 0 & 0 & 0 \\
0.006 & 0.007 & 0.325 & 0.231 & 0.431 & 0 & 0 & 0 \\
0.002 & 0.003 & 0.137 & 0.179 & 0.099 & 0.420 & 0.116 & 0.044 \\
0.002 & 0.003 & 0.125 & 0.097 & 0.158 & 0.385 & 0.167 & 0.064 \\
0.001 & 0.001 & 0.050 & 0.059 & 0.043 & 0.154 & 0.500 & 0.192 \\
0.001 & 0.002 & 0.085 & 0.107 & 0.066 & 0.260 & 0.346 & 0.133 \\
0.001 & 0.002 & 0.067 & 0.083 & 0.054 & 0.207 & 0.423 & 0.163 \\
0.001 & 0.001 & 0.048 & 0.045 & 0.053 & 0.148 & 0.231 & 0.473 \\
0.001 & 0.002 & 0.079 & 0.066 & 0.095 & 0.243 & 0.205 & 0.310 \\
0.001 & 0.002 & 0.063 & 0.055 & 0.074 & 0.195 & 0.218 & 0.392
\end{bmatrix}$$

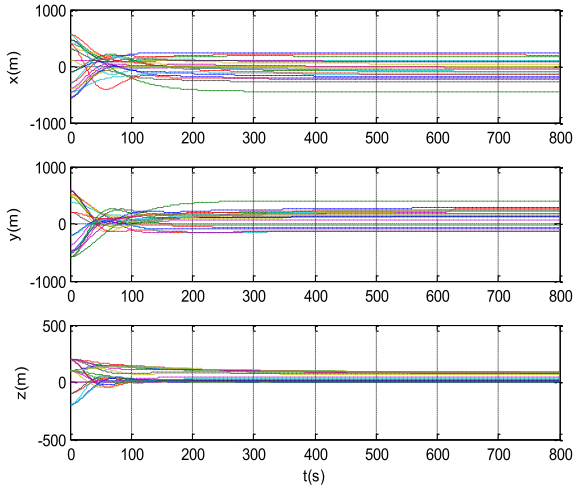

(a) Position trajectories for each follower

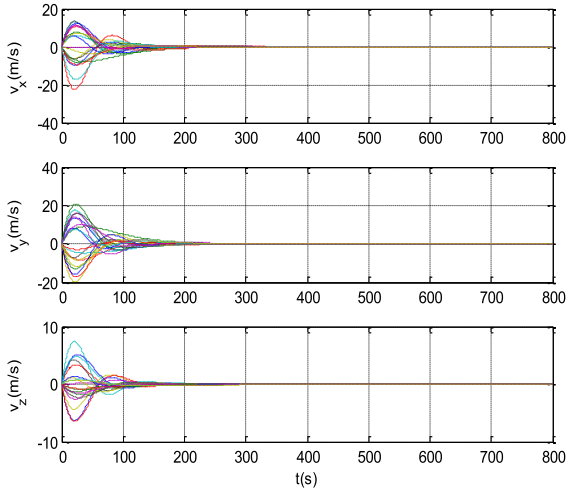

(b) Velocity trajectories for each follower

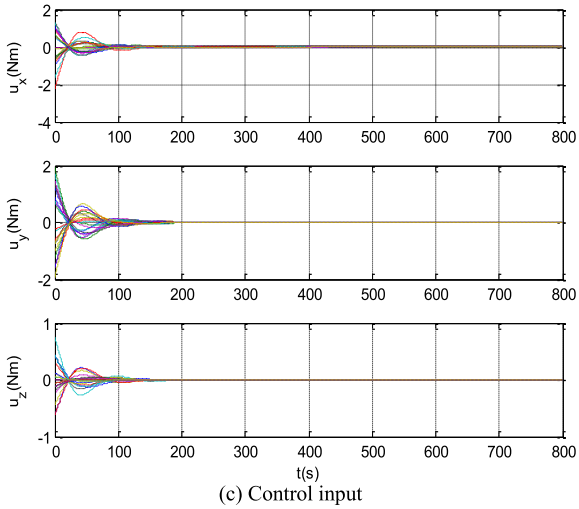

(c) Control input

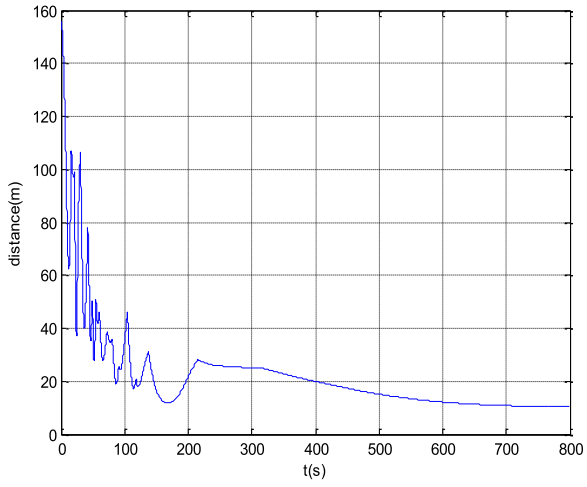

(d) The shortest distance among followers

FIGURE 12. **Simulation results with Fig.11 as information topology.**

The variable weight coefficient can be guaranteed if $\left\|\left(r_i - r_j\right) - \left(r_i^d - r_j^d\right)\right\| > \left(\delta + \left\|r_i^d - r_j^d\right\|\right)$ is satisfied at initial time. That is, under the control of controller (25), $\left\|r_i - r_j\right\| > \delta$, there are no collisions between members. However, the principle of variable weight coefficient method lies in: When the distance between neighbors approaches a certain value, the system will suddenly increase control force to increase the distance between neighbors, thus collisions are prevented. However, due to the obvious increase of control force in the process of collision avoidance, if the actual output control force of spacecraft cannot meet the requirements, the collision avoidance function may fail.

The potential function method is simulated as follows. For simplicity, consider the case where there are only two member spacecraft, and assume that two spacecraft can obtain relative position information of each other. The initial position,velocity and desired position of the two spacecraft in reference orbit coordinate system respectively are

$$\boldsymbol{r}_1 = [430, 330, 210]^{\mathrm{T}} m \quad \dot{\boldsymbol{r}}_1 = [-0.6, -0.8, -0.7]^{\mathrm{T}} m/s$$
$$\boldsymbol{r}_2 = [385, 355, 145]^{\mathrm{T}} m \quad \dot{\boldsymbol{r}}_2 = [0.5, -0.7, 0.6]^{\mathrm{T}} m/s$$

$$\boldsymbol{r}_1^d = [420, 350, 200]^{\mathrm{T}} m$$
$$\boldsymbol{r}_2^d = [410, 340, 180]^{\mathrm{T}} m$$

Safe collision avoidance distance $\delta = 10m$.
Control parameters are set as

$$\alpha = 0.1, \beta = 0.01, a_{12} = 0.0001, a_{21} = 0.0001$$

Simulation results are shown as Fig.13. It can be seen from Fig.13(a) and Fig.13(b) that the two spacecraft will converge to the desired state, and the shortest distance between spacecraft is always more than 10 meters in simulation process(Fig.13(d)), so collisions will not collide. According to Fig.13(c), contol force of spacecraft 1 will suddenly and sharply increase in 8-9s, and control foce of spacecraft 2 will increase in about 15s, which is caused by variable weight coefficient closing to 0.

Compare with variable weight coefficient method, the problem of excessive control force in collision avoidance can be solved with rationally designing cluster information topology. Control force and convergence rate can be

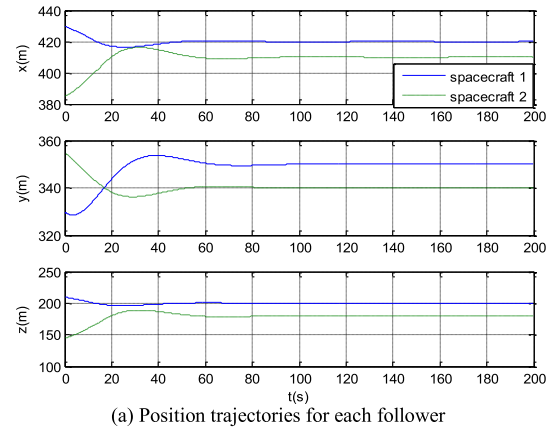

(a) Position trajectories for each follower

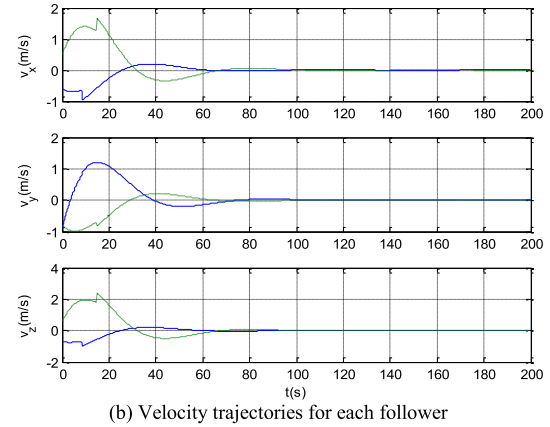

(b) Velocity trajectories for each follower

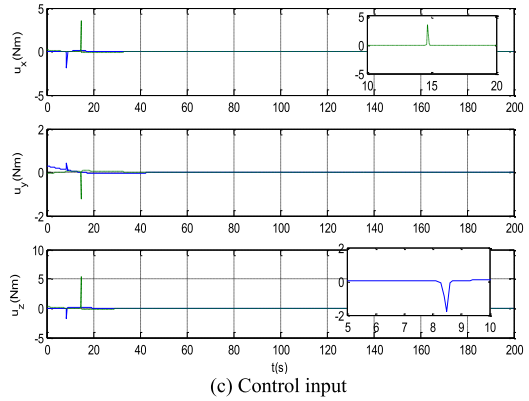

(c) Control input

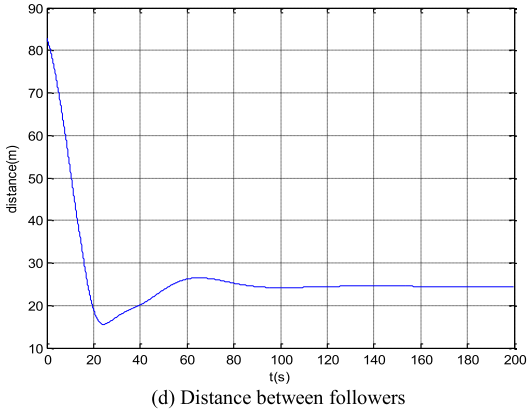

(d) Distance between followers

FIGURE 13. Simulation results of potential function method.

adjusted in a reasonable range by using theory analysis in Section III.

VI. CONCLUSION

This paper mainly studied coordinated orbit control problem for large-scale cluster spacecraft system in the view of information topology. A distributed orbital containment control algorithm was given for large-scale cluster spacecraft system to drive all followers into the convex hull formed by leaders. The influence of information topology and control gain coefficient on convergence and convergence rate of cluster system was analyzed. All followers' steady states for containment control were investigated from graph theory. Main research content of this paper is shown as follows:

1) For large-scale cluster flying spacecraft with leader-follower architecture, a general distributed orbital containment control algorithm was given. The primary constraint condition for containment control on cluster information topology was that each follower can be reached from at least one leader. The influence of information topology on convergence and convergence rate of cluster system was also analyzed, providing a theoretical reference for information topology design which aims at improving the convergence rate of the system. Simulation examples have been provided, which showed the effectiveness of information topology constraints.

2) The influence of control gain coefficient on system convergence and convergence rate have been analyzed based on graph theory. The formula of control gain coefficient which make system to obtain maximum convergence rate was given based on the eigenvalues of cluster Laplacian matrix, providing methods for how to obtain a satisfactory convergence rate using less control force. Numerical simulations have been carried out to verify the validity of theory analysis.

3) The followers' steady states for containment control were investigated from graph theory. It was shown that the steady state of each follower is influenced by the leaders that can reach it, and two kinds of cell partitions were defined to characterize system information topologies with the property that the followers which belong to the same cell had the same steady state, providing methods for how to avoid collisions.

For large-scale cluster satellite flight missions, the problems to be considered consist of external disturbance, model disturbances, time-delay, etc. Initial state error and various perturbation factors will cause the formation configuration to drift, and satellite faults(such as thruster fault, sensor fault, etc). Further the aforementioned problems in large-scale cluster spacecraft will be discussed.

REFERENCES

[1] O. Ben-Yaacov, A. Ivantsov, and P. Gurfil, "Covariance analysis of differential drag-based satellite cluster flight," *Acta Astronaut.*, vol. 123, pp. 387–396, Jun. 2016.

[2] J. Luo, L. Zhou, and B. Zhang, "Consensus of satellite cluster flight using an energy-matching optimal control method," *Adv. Space Res.*, vol. 60, no. 9, pp. 2047–2059, Nov. 2017.

[3] W. Zhong, "Research on the orbit navigation and control of the satellite cluster," Ph.D. dissertation, HIT, Harbin, China, 2014.

[4] H. Zhang and P. Gurfil, "Distributed control for satellite cluster flight under different communication topologies," *J. Guid., Control, Dyn.*, vol. 39, no. 3, pp. 1–11, Jul. 2015.

[5] E. Vassev and M. Hinchey, "Self-awareness in autonomous nano-technology swarm missions," in *Proc. 5th IEEE Conf. Self-Adapt. Self-Organizing Syst. Workshops*, Oct. 2011, pp. 133–136.
[6] Z. Li, L. Guo, J. Huang, X. Zhang, and B. Zhang, "Study on development status of light sail spacecraft and key technologies of breakthrough starshot project," *Spacecraft Eng.*, vol. 25, no. 5, pp. 111–118, 2016.
[7] Y. Zhao, P. Gurfil, and S. Zhang, "Long-term orbital dynamics of smart dust," *J. Spacecraft Rockets*, vol. 55, no. 1, pp. 125–142, Jan. 2018.
[8] J. R. Lawton and R. W. Beard, "Synchronized multiple spacecraft rotations," *Automatica*, vol. 38, no. 8, pp. 1359–1364, Aug. 2002.
[9] H. Liang, Z. Sun, and J. Wang, "Robust decentralized attitude control of spacecraft formations under time-varying topologies, model uncertainties and disturbances," *Acta Astronautica*, vol. 81, no. 2, pp. 445–455, Dec. 2012.
[10] H. Du, M. Z. Q. Chen, and G. Wen, "Leader-following attitude consensus for spacecraft formation with rigid and flexible spacecraft," *J. Guid. Control Dyn.*, vol. 39, no. 4, pp. 1–8. Jan. 2016.
[11] H. Cai and J. Huang, "Leader-following attitude consensus of multiple rigid body systems by attitude feedback control," *Automatica*, vol. 69, pp. 87–92. Jul. 2016.
[12] L. Shi, J. Shao, W. X. Zheng, and T.-Z. Huang, "Asynchronous containment control for discrete-time second-order multi-agent systems with time-varying delays," *J. Franklin Inst.*, vol. 354, no. 18, pp. 8552–8569, Dec. 2017.
[13] M. Ji, G. Ferrari-Trecate, M. Egerstedt, and A. Buffa, "Containment control in mobile networks," *IEEE Trans. Autom. Control*, vol. 53, no. 8, pp. 1972–1975, Sep. 2008.
[14] X. Dong, Y. Hua, Y. Zhou, Z. Ren, and Y. Zhong, "Theory and experiment on formation-containment control of multiple multirotor unmanned aerial vehicle systems," *IEEE Trans. Autom. Sci. Eng.*, vol. 16, no. 1, pp. 229–240, Jan. 2019.
[15] H. Qin, H. Chen, Y. Sun, and Z. Wu, "The distributed adaptive finite-time chattering reduction containment control for multiple ocean bottom flying nodes," *Int. J. Fuzzy Syst.*, vol. 21, no. 2, pp. 607–619, Mar. 2019.
[16] Y. Sun, G. Ma, M. Liu, and L. Chen, "Distributed finite-time configuration containment control for satellite formation," *Proc. Inst. Mech. Eng. G, J. Aerosp. Eng.*, vol. 231, no. 9, pp. 1609–1620, Jul. 2017.
[17] Y. Sun, G. Ma, L. Chen, and P. Wang, "Neural network-based distributed adaptive configuration containment control for satellite formations," *Proc. Inst. Mech. Eng. G, J. Aerosp. Eng.*, vol. 232, no. 12, pp. 2349–2363, Sep. 2018.
[18] Y. Cao and W. Ren, "Containment control with multiple stationary or dynamic leaders under a directed interaction graph," in *Proc. 48h IEEE Conf. Decis. Control (CDC) Held Jointly 28th Chin. Control Conf.*, Piscataway, NJ, USA, Dec. 2009, pp. 3014–3019.
[19] G. Notarstefano, M. Egerstedt, and M. Haque, "Containment in leader–follower networks with switching communication topologies," *Automatica*, vol. 47, no. 5, pp. 1035–1040, May 2011.
[20] Y. Cao, D. Stuart, W. Ren, and Z. Meng, "Distributed containment control for multiple autonomous vehicles with double-integrator dynamics: Algorithms and experiments," *IEEE Trans. Control Syst. Technol.*, vol. 19, no. 4, pp. 929–938, Jul. 2011.
[21] A. Zhang, C. Jian, and K. Xianren, "Containment control protocol and its convergence speed analysis for double-integrator dynamics systems," *J. Harbin Inst. Technol.*, vol. 46, no. 9, pp. 1–8, Sep. 2014.
[22] K. Liu, G. Xie, and L. Wang, "Containment control for second-order multi-agent systems with time-varying delays," *Syst. Control Lett.*, vol. 67, pp. 24–31, May 2014.
[23] Z. Meng, W. Ren, and Z. You, "Distributed finite-time attitude containment control for multiple rigid bodies," *Automatica*, vol. 46, no. 12, pp. 2092–2099, Dec. 2010.
[24] J. Mei, W. Ren, and G. Ma, "Distributed containment control for Lagrangian networks with parametric uncertainties under a directed graph," *Automatica*, vol. 48, no. 4, pp. 653–659, Apr. 2012.
[25] A. Zhang, X. Kong, S. Zhang, and F. Wang, "Distributed attitude cooperative control with multiple leaders," *J. Harbin Inst. Technol.*, vol. 45, no. 3, pp. 1–6, Mar. 2013.
[26] S. Zuo, Y. Song, F. L. Lewis, and A. Davoudi, "Time-varying output formation containment of general linear homogeneous and heterogeneous multiagent systems," *IEEE Trans. Control Netw. Syst.*, vol. 6, no. 2, pp. 537–548, Jun. 2019.
[27] T. Xu, Y. Hao, and Z. Duan, "Fully distributed containment control for multiple Euler–Lagrange systems over directed graphs: An event-triggered approach," *IEEE Trans. Circuits Syst. I, Reg. Papers*, vol. 67, no. 6, pp. 2078–2090, Jun. 2020.
[28] L. Chen, Y. Guo, C. Li, and J. Huang, "Satellite formation-containment flying control with collision avoidance," *J. Aerosp. Inf. Syst.*, vol. 15, no. 5, pp. 253–270, 2018.
[29] B. Owen, "Fractionated spacecraft workshop: Vision and objectives," in *Proc. DARPA Fractionated Spacecraft Workshop*, Colorado Springs, CO, USA, Aug. 2006, pp. 1–15.
[30] H. Min, C. Haiping, and Z. Guoqiang, "Cyclic pursuit control for fractionated spacecraft formation reconfiguration using local information only," in *Proc. 24th Chin. Control Decis. Conf. (CCDC)*, May 2012, pp. 1437–1441.
[31] M. B. Quadrelli, S. Basinger, and G. Swartzlander, "Multi-scale dynamics, control, and simulation of granular spacecraft," in *Proc. Eur. Netw. Social Emotional Competence*, Zagreb, Croatia, 2013, pp. 1–8.
[32] K. Lerman, A. Martinoli, and A. Galstyan, "A review of probabilistic macroscopic models for swarm robotic systems," in *Proc. Int. Workshop Swarm Robot.* Berlin, Germany: Springer, 2004, pp. 143–152.
[33] M. B. Quadrelli, S. Basinger, and D. Arumugam. (2017). Orbiting Rainbows: Future Space Imaging With Granular Systems. JPL, California Institute of Technology. [Online]. Available: https://ntrs.nasa.gov/search.jsp?R=20170004834
[34] A. Zhang, J. Chen, S. Zhang, X. Kong, and F. Wang, "Graph-theoretic characterisations of the steady states for containment control," *Int. J. Control*, vol. 85, no. 10, pp. 1574–1580, Oct. 2012.
[35] S. Martini, M. Egerstedt, and A. Bicchi, "Controllability analysis of multi-agent systems using relaxed equitable partitions," *Int. J. Syst., Control Commun.*, vol. 2, nos. 1–3, pp. 100–121, 2010.
[36] A. Aggarwal, J. S. Chang, and C. K. Yap, "Minimum area circumscribing polygons," *Vis. Comput.*, vol. 1, no. 2, pp. 112–117, Aug. 1985.
[37] J. Zhu, Y. Tian, and J. Kuang, "On the general consensus protocol of multi-agent systems with double-integrator dynamics," *Linear Algebra Appl.*, vol. 431, nos. 5–7, pp. 701–715, 2009.
[38] X. Zhang, *The Analysis and Application of Matrix*. Beijing, China: Tsinghua Univ. Press, 2004.
[39] J. S. Caughman and J. J. P. Veerman, "Kernels of directed graph Laplacians," *Electron. J. Combinatorics*, vol. 13, no. 1, pp. 1–8, Apr. 2006.
[40] F. Zhang, S. Zhang, Y. Zhang, H. Guo, and A. Zhang, "Consensus-based distributed control of multi-agent systems," in *Proc. 1st Int. Conf. Pervas. Comput., Signal Process. Appl.*, Sep. 2010, pp. 216–219.

SHIJIE ZHANG received the B.S., M.S., and Ph.D. degrees in spacecraft design from the Harbin Institute of Technology, Harbin, China, in 2000, 2002, and 2005, respectively.

He is currently a Professor with the Research Center of Satellite Technology, Harbin Institute of Technology. He has been a Principal Investigator of over 30 research and development projects related to small satellites, with current projects focusing on orbital and attitude dynamics of small satellites and formation flying, and vision-based satellite navigation. He was involved in the development of three small satellites. His research interests include the dynamics and control of satellites and formation flying, and the space mission analysis and design of small satellites.

Dr. Zhang was a recipient of the Royal Academy of Engineering Research Exchanges with China and India Award–Major Award to study autonomous control and operation of spacecraft formation using software and hardware technology.

FENGZHI GUO received the B.S. degree in aircraft design and engineering and the M.S. degree in aeronautical and astronautical science and technology from Harbin Engineering University, Harbin, China, in 2013 and 2016, respectively. She is currently pursuing the Ph.D. degree in aeronautical and astronautical science and technology with the Harbin Institute of Technology, Harbin.

Her research interests include dynamics modeling and control of satellites, and coordinated attitude and orbit control of cluster spacecraft.

ANHUI ZHANG received the B.S. degree from Shandong Normal University, Jinan, China, in 2004, the M.S. degree from Capital Normal University, Beijing, China, in 2007, and the Ph.D. degree in aeronautical and astronautical science and technology from the Harbin Institute of Technology, Harbin, China, in 2013.

TINGTING ZHANG received the B.S. degree in mathematics and applied mathematics from Shangqiu Normal University, Shangqiu, China, in 2015, and the M.S. degree in mathematics from Heilongjiang University, Harbin, China, in 2018. She is currently pursuing the Ph.D. degree in aeronautical and astronautical science and technology with the Harbin Institute of Technology, Harbin.

Her research interests include numerical analysis of Volterra integral equations and coordinated attitude and orbit control of spacecraft.